JOURNAL OF MATERIALS SCIENCE 33 (1998) 3763–3783

Review
Shape memory materials and hybrid composites for smart systems
Part II *Shape-memory hybrid composites*

Z. G. WEI, R. SANDSTRÖM
Department of Materials Science and Engineering, Royal Institute of Technology, S-10044, Stockholm, Sweden
E-mail: ZGWEI@kth.se

S. MIYAZAKI
Institute of Materials Science, University of Tsukuba, Tsukuba, Ibaraki 305, Japan

By hybridizing or incorporating shape-memory materials with other functional materials or structural materials, smart composites can be fabricated which may utilize the unique functions or properties of the individual bulk materials to achieve multiple responses and optimal properties, or, to tune their properties to adapt to environmental changes. A variety of shape-memory hybrid composites have been designed and manufactured, with shape-memory elements being either the matrix or the reinforcement. The hybrid composites provide tremendous potential for creating new paradigms for material–structural interactions and demonstrate varying success in many engineering applications. This review, from the standpoint of materials science, will give a state-of-the-art survey on the various shape-memory hybrid smart composites developed during the last decade. Emphasis is placed on the design, fabrication, characterization and performance of fibre-reinforced, particle-reinforced and multi-layered thin-film shape-memory composites.

1. Introduction

In 1988, Rogers and co-workers at Virginia Tech embarked on their research and development efforts of smart/intelligent materials and structures, which have now gained world-wide attention [1– 4]. One of their main efforts was to utilize the novel performance of shape-memory materials, such as high damping capacity, large recoverable strain and recovery stress, and remarkable property changes due to thermal or stress-induced martensitic transformations, to engineer hybrid intelligent composites natively with "multi-functionality" or adaptive properties [1, 2, 5–8]. In the approaches, shape-memory materials were usually integrated within monolithic or composite host materials to produce the desired components whose functionality or static and dynamic properties could be enhanced or actively tuned in response to environmental changes. The shape-memory hybrid composites, with either embedded or bonded shape-memory material components, have proved to be unique material systems that provide tremendous potential for creating new paradigms for material-structural interaction [5]. Owing to the intriguing characteristics and exciting potentials in engineering applications, shape-memory hybrid composites have emerged as one of the promising smart material systems and hence been the subject of active investigation during the past decade [1, 4–8].

Commerical shape-memory materials can be easily fabricated into various forms such as fibres, wires, ribbons, particles and thin films, therefore making it feasible to manufacture a great diversity of shape-memory hybrid composites with conventional fabrication procedures [9]. As usual, both continuously reinforced composites with fibre or film reinforcements and discontinuously reinforced composites with particulate or flake reinforcements, have been designed and fabricated, with shape-memory elements being either the reinforcement or the matrix. Partly due to the technical simplicity in manufacturing, most of previous efforts with embedded shape-memory fibres or wires have been directed at thermoplastic and thermoset polymer matrix composites, and many engineering applications have been found for the smart composites [5–8]. For instance, the polymer matrix shape-memory composites have demonstrated varying success in the fields including: shape and position control, active and passive control of the vibration and acoustic transmission of materials subjected to dynamic loads, impact damage and creep resistance

in structures [3, 8]. More recently, the engineering approaches to design and fabrication of intelligent composites using shape-memory materials have been extended to metal or silicon matrices: shape-memory alloy ribbons or filaments can be embedded within silicon layers of variable thickness to form composite laminates with controllable stiffness and improved shape-memory performance [10–12]; some unique properties such as self-strengthening or self-relaxation and high damping capacity may be achieved in metal matrix composites containing shape-memory alloy fibres or particles [13–15].

In the first part of the review [9], we outlined shape-memory materials and their basic characteristics. In this part we will give a state-of-the-art survey of the smart/intelligent composites based on shape-memory materials. The main achievements during the past decade will be summarized, with an emphasis on the design concept, fabrication, characterization and performance of the composites.

2. Fibre-reinforced shape-memory composites

2.1. Shape-memory alloy fibre/metal matrix composites

2.1.1. Material design

Owing to the mismatch of the thermal expansion coefficient (CTE) between the matrix and filler, a tensile or compressive residual thermal stress will be introduced into the composite when fabricated at high temperature and then cooled down to room temperature. It is well established that compressive residual stress in the matrix, caused by a higher CTE of the filler than that of the matrix, is beneficial to mechanical properties such as the yield stress and fracture toughness. If there is a special filler that shrinks in the matrix at the temperature of operation or with increasing applied stress, compressive stress may also be introduced into the matrix, thereby contributing to the tensile properties of the composite. Shape-memory alloys (SMAs) do exhibit such shrinkage when prestrained at martensite state and then heated to the parent phase state. Taking into account that SMA fibres are easily fabricated and have a high strength, good ductility, high damping and fatigue resistance, they are interesting reinforcement candidates. If such shrinkable SMA fibres are embedded in metals and alloys to form metal matrix composites (MMCs), a compressive residual stress may be generated in the matrix and hence the tensile flow stress of the MMCs is expected to be enhanced. In addition, the adaptive mechanisms such as self-repairing of damage, i.e. microcrack closure, and the suppression effect for fatigue crack propagation may be operative. As a result, the fracture toughness and fatigue resistance of the composites may be improved.

In the light of the mechanism, Furuya *et al.* [14–17] have proposed the design concept of Ti–Ni fibres-reinforced aluminium matrix composites. The basic design approaches for the SMA fibremetal matrix composite can be summarized as a five-step route as shown in Fig. 1: the SMA fibremetal matrix composites are prepared and fabricated by using conventional fabrication techniques; (2) the as-fabricated composites are heated to high temperatures to shape memorize the fibres or to undergo some specific heat treatment for the matrix material, if necessary; (3) because SMAs have much lower stiffness at the martensite stage or readily yield at the austenitic stage just above the martensitic transformation start temperature, M_s, the composites are then cooled to lower temperatures, preferably in the martensite state; (4) the composites are further subjected to proper deformations at the lower temperature to enable the martensite twinning or the stress-induced martensitic transformation to occur; and (5) the prestrained composites are then heated to higher temperatures, preferably above the austenite finish temperature, A_f, wherein martensite detwinning or the reverse transformation from martensite to austenite takes place and the Ti–Ni fibres will try to recover their original shapes and hence tend to shrink, introducing compressive internal residual stresses in the composites. This design concept can also be applied to polymer matrix composites containing SMA fibres and to the metal matrix composites containing SMA particles.

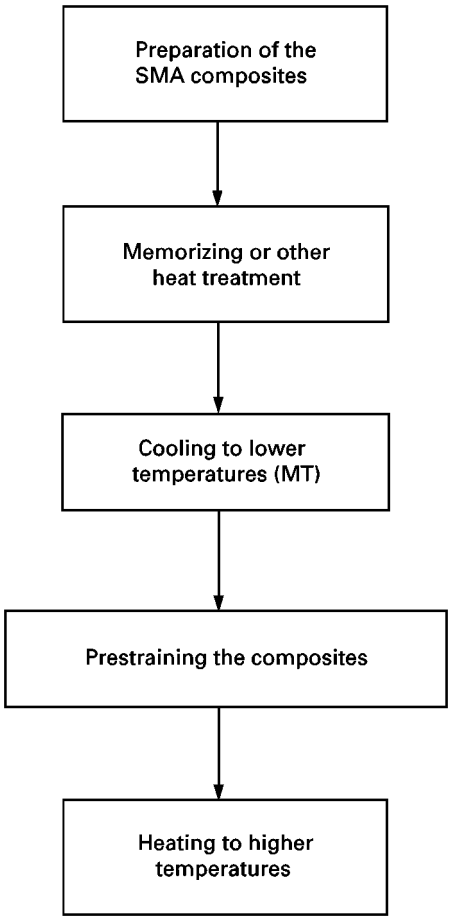

Figure 1 Design concept of SMA-reinforced composites

2.1.2. Manufacturing procedures

The excellent ductility and workability of Ti–Ni SMAs make it very easy to fabricate fibres of several hundred micrometres in diameter with conventional

processing methods. Embedding the fibres in the aluminium matrix can be achieved by squeeze casting or compacting via a powder metallurgical route. Specially, three kinds of fabrication procedures have been developed.

(a) The Ti–Ni fibres were arranged in a fixed holder in a mould, then molten aluminium (970 K) was poured into the mould, followed by pressurization at 65 MPa. Because the melting temperature of aluminium is not very high, even though a thin layer with a thickness of less than 3 μm of the fibre surface was affected by diffusion interaction, most of the Ti–Ni fibres remained unaffected during the processing. The composite was then subjected to heat treatment (773 K, 30 min) to shape memorize the Ti–Ni fibres, followed by ice–water quenching to induce martensitic transformation. A specific tensile prestrain was applied and then the composite was heated to a temperature above the A_f point [14].

(b) Aluminium powders and Ti–Ni fibres were placed in a mould and were pressed at 200 MPa in air at room temperature to form a green sheet, and then it was sintered in a vacuum furnace (10^{-4} torr) at 843 K for 1 h. Simultaneously, a shape-memory treatment was made during the sintering process. The porosity of the as-sintered composite was 8%. The high elongation of the aluminium matrix at room temperature (up to 12%) would provide prestrains of up to 4%–5% to the Ti–Ni fibres [15, 17]. Because pure aluminium (Al–1100) has a too low flow stress to be used as a matrix metal in many structural composite applications, more recently, 6061-T6 and 6082-T6 aged aluminium alloys with a higher yield stress were used as the metal matrix of the shape-memory fibre-enhanced composite [18, 20, 21].

(c) The Ti–Ni fibres were wound around or longitudinally laced on to thin aluminium alloy sheet with rectangular end notches. The fibre-laced prepreg sheets were stacked on a pair of hot-press dies or loaded into a vacuum cannister and then were hot pressed at proper temperatures and pressures, as illustrated in Fig. 2. A thin layer (within 3 μm) of interfacial phases such as Al_3Ti and Al_3Ni was produced because of the interfacial reactions between the Ti–Ni fibre and the matrix. The optimum vacuum hot-pressing conditions for Al-6061 matrix composite were found to be 773 K for 30 min at 54 MPa [21]. The material could be either directly water quenched and then aged, or cooled down in the furnace while keeping the pressure constant, followed by a solution treatment and T6 ageing. A loading and unloading process was applied to the composite at room temperature to produce various prestrains. This processing procedure resulted in good macro-scale homogeneity and little internal porosity, and various volume fractions of Ti–Ni fibres could be embedded into the aluminium matrix [18, 20, 21].

More recently, Mizuuchi *et al.* [22] also prepared Ti–Pd–Ni–W SMA fibre titanium matrix composites by sheath-rolling: the Ti–Pd–Ni–W SMA fibres were laminated between titanium plates, and inserted into a stainless pipe and vacuum encapsuled, then the sealed laminates were sheath-rolled at the temperatures between 1123 and 1223 K, followed by reheating at the temperatures for different times. A reaction interfacial layer with a thickness of about 30 μm and composed of three different intermetallic compounds was formed between the fibres and the matrix. The interfacial layer was found to be effective for stress conductivity.

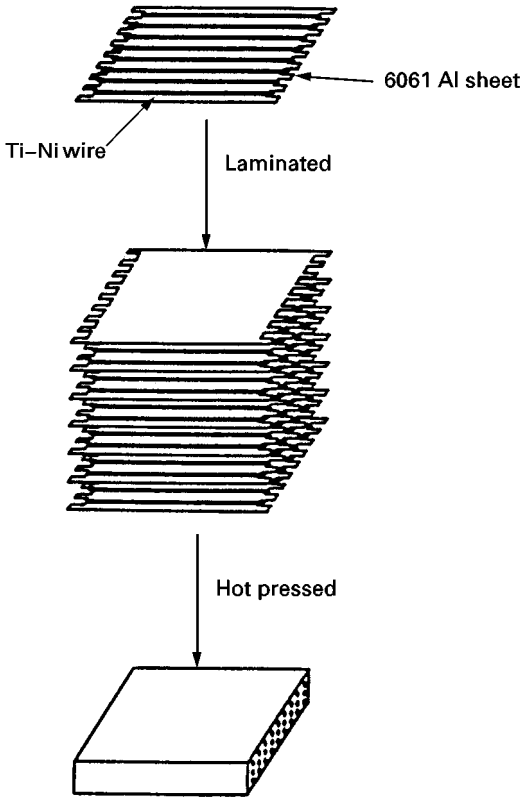

Figure 2 Fabrication procedure of SMA wire wound prepreg [21].

2.1.3. Materials properties

The internal residual stress in both the fibre and the matrix, and the composite macroscopic strains as a function of external variables such as temperature and applied load or prestrain have been calculated within non-linear composite models using Eshelby's formulation [17–19, 21]. As expected, depending on the fibre pre-treatment and distribution, as well as the boundary conditions, varying levels of compressive residual stresses can be generated in the matrix of the SMA composite during the heating process, resulting in a large negative thermal expansion [18, 19]. For a given SMA fibre reinforcement, the matrix compressive residual stress increases with increasing volume fraction and prestrain of the SMA fibres within a limited range, and optimal prestrain and fibre volume fraction values can be found [17]. In addition, the magnitude of the internal residual stress is also limited by the flow strength of both the SMA fibres and the matrix materials. Once the residual stresses in the matrix and fibres are determined, the yield stress of the composite can be obtained from the stress–strain curve defined by [17].

$$\sigma_o = \sigma_y + He_p \quad (1)$$

where σ_y and H are the tensile yield stress and working hardening rate of the composite, respectively, e_p is the plastic strain, and σ_0 is related to the residual stress in the form

$$\sigma_0 = \sigma_{ym} + \frac{V_f}{1 - V_f}(\sigma_{33} - \sigma_{11}) \quad (2)$$

where σ_{ym} is the yield stress of the matrix, V_f the volume fraction of SMA fibres, and $(\sigma_{33} - \sigma_{11})$ is the disturbance stress. Apart from the dependence on the volume fraction and prestrain, the yield stress of the composite also increases with increasing temperature within a limited temperature range [19]. This is because the contributing back stress in the aluminium matrix induced by stiffness of Ti–Ni fibres and the compressive stress in the matrix originate from the reverse transformation process from the "soft" martensite to the parent phase (austenite) with a several times higher stiffness. For the austenite phase fibre, the critical stress to induce the martensitic transformation shows a strong positive dependence on temperature, as demonstrated in the Clausius–Clapeyon equation and temperature–stress–strain curves of SMAs [9].

Experimental results have confirmed the theoretical predictions. A 19.5 vol % Ti–Ni fibre-reinforced 6061-T6 aluminium alloy matrix composite exhibited an unusual non-linear thermal contraction during unconstrained heating from 298–348 K, implying that a compressive internal stress must have developed [18]. *In situ* X-ray diffraction and neutron diffraction measurements are being performed to determine further the transformation processes. Some preliminary results have shown that the macroscopic broad yield point region in the tensile process indeed corresponds to the transformation from the B2 austenite to B19′ martensite [20]. In the tensile tests at room temperature, the TiNi/6061-T6 composite exhibited an initial elastic response followed by a bimodal yield, with only a slight increase in the flow strength over the monolithic aluminium alloy (from 280 MPa to about 310 MPa). However, an unusual, positive curvature flow-hardening rate was observed during the final stages of loading, due to the saturation of the stress-induced transformation. At a higher temperature (348 K), although there was a low initial yield with a much smaller decrease in tangent modulus than the case at room temperature, the composite exhibited a full yield stress of about 390 MPa with positive curvature hardening in the strain range of interest. The final failure strain of the composite exceeded 15%. Both the ultimate strength and the failure strain of the composite were significantly greater than those of the unreinforced 6061-T6 control material [18].

In agreement with modelling predictions, with increasing fibre volume fraction and prestrain, a more significant strengthening effect of the composite by the SMA fibres was observed [14, 21]. The stress–strain curves of the composite with 1100 pure aluminium matrix and varying volume fraction of Ti–Ni fibres were measured, and it was found that the Young's modulus and tensile yield stress increase with increasing volume fraction of fibres [14]. The yield stress of the Al-1100 matrix composite with 9% volume fraction of 4.0% prestrained Ti–Ni fibres was increased by approximately 100% over the pure aluminium, as shown in Fig. 3. The effect of prestrain on the yield stress is demonstrated in Fig. 4. In the 3 vol % TiNi fibres/Al-1100 composite, the yield stress increased from 39.5 MPa to 64.8 MPa when prestrain was increased from 0 to 1.5% [17]. For the 6061 Al matrix composite with 2.7 vol % TiNi fibres, the yield stress, σ_y, and the amount of prestrain, ε_p, can be roughly expressed by the following linear relationships, depending on the heat-treatment condition [21]

$$\sigma_y = 15.677\ \varepsilon_p + 283.15 \quad \text{with T6 ageing treatment} \quad (3)$$

$$\sigma_y = 18.719\ \varepsilon_p + 77.599 \quad \text{without T6 ageing treatment} \quad (4)$$

On the other hand, the prestrain generally contributes to the damage accumulation for failure and it works to decrease the elognation and ductility of the composites [15]. The effect of SMA fibre volume fraction and prestrain on the yield stress at various temperatures for Ti–Pd–Ni–W SMA fibre/Ti matrix

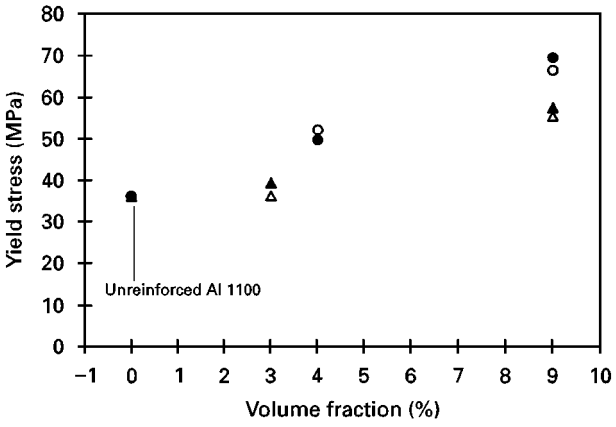

Figure 3 Dependence of yield stress on SMA fibre volume fraction for the TiNi/A1 1100 composite (▲, ●) experimental data, (△, ○) Theoretical calculations were based on the Eshelby's formulation. Prestain: (△, ▲) 0%, (○, ●) 4%. Data sources [16, 17].

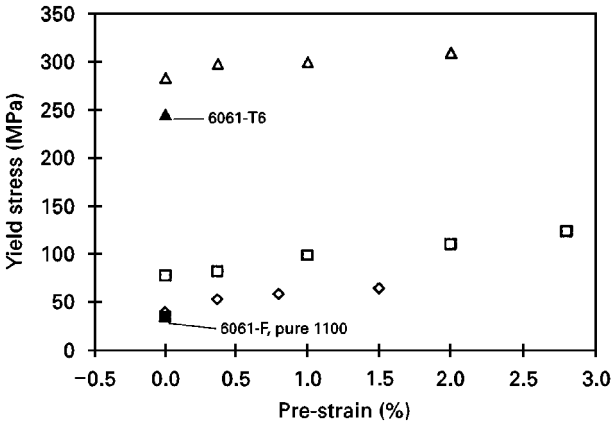

Figure 4 Dependence of yield stress on prestrain for (◇) TiNi/Al 1100 composite and TiNi/Al 6061 composites (△) with and (□) without T6 ageing treatment [17, 21]. The value for the corresponding pure aluminum material were depicted.

composites were also examined, and varying amount of increase in the yield strength of the composites were also examined, and varying amount of increase in the yield strength of the composites as compared to the monolithic titanium was observed [22].

The crack propagation rate as a function of the apparent stress intensity factor in the composites was measured by Furuya [15, 17]. A drastic drop of the propagation rate, i.e. crack-closure effect, was observed after the composite was heated to higher temperatures ($> A_f$). The enhancement of the resistance to fatigue crack propagation was suggested to be ascribed to the combination of compressive residual stress, higher stiffness of the composite, the stress-induced martensitic transformation and the dispersion of the mechanical strain energy at the crack tip [15]. Olson *and co-workers* [23] have been attempting to design a biomimetric self-heating "smart steel" composite consisting of a B2-strengthened ferritic superalloy reinforced by a thermodynamically compatible, second-phase (γ')-strengthened austenitic shape-memory alloy, using the martensitic transformation as a toughening mechanism. In their exploratory experiments, Ti– 42.7 wt % Ni–11.7 wt % Cu shape-memory wires of a 200 μm diameter were used as the fibre reinforcement in an Sn–Bi matrix. It was found that stable macrocracks were clamped shut due to the reverse martensitic transformation [23]. The SMA fibre-reinforced MMCs also exhibit other improved properties. For instance, the damping capacity of the Ti–Ni fibre Al matrix composite was measured by using a uniaxial vibration method, and the results indicated that the damping capacity (tan δ) of the composite in the temperature range 270–450 K was substantially improved over the unreinforced aluminium [14]. The composite was also expected to show high wear resistance [14, 15]. The encouraging results as shown in the above-mentioned approaches suggest that more detailed investigations and systematic evaluation of the overall properties of the SMA fibres-reinforced metal matrix composites are needed.

2.2. Shape-memorey alloy fibre/polymer matrix composites

2.2.1. Design considerations

Depending on the SMA fibre pretreatment, distribution configuration and host matrix material, a variety of hybrid polymer matrix composites can be designed which may actively or passively control the static and/or dynamic properties of composite materials. Passively, as in the SMA fibre Al matrix composites, the shape-memory alloy fibres are used to strengthen the polymer matrix composites, to absorb strain energy and alleviate the residual stress and thereby improve the creep or crack resistance by stress-induced martensitic transformations. Actively, the embedded SMA fibres are usually activated by electric current heating and hence undergo the reverse martensitic transformation, giving rise to a change of stiffness, vibration frequency and amplitude, acoustic transmission or shape of the composite. As a result, structural tuning, modal modification or vibration and acoustic control can be accomplished through: (i) the change in stiffness (inherent modulus) of the embedded SMA elements or, (ii) activating the prestrained SMA elements to generate a stress (tension or compression) which will tailor the structural performance and modify the modal response of the whole composite system just like tuning a guitar string. The two techniques are termed as "active property tuning" (APT) and "active strain energy tuning" (ASET), respectively [7, 8, 24]. In general, APT requires a large volume fraction of SMA fibres that are embedded without prior plastic elongation and do not create any large internal forces. However ASET may be equally effective with an order of magnitude smaller volume fraction of SMA fibres that are "active", and impart large internal stresses throughout the structure [24].

Usually, the embedded or bonded shape-memory alloy fibres should be plastically elongated and constrained from contracting to their "normal" length before they are cured to become an integral part of the material. When the fibres are activated by passing a current through them, they will try to contract to their normal length and therefore generate a large, uniformly distributed shear load along the length of the fibres. The shear load then alters the energy balance within the structure and therefore changes its modal response [5, 8, 24]. Shape-memory alloy fibres can also be embedded in a material off the neutral axis on both sides of the beam in an antagonist–anti-antagonist pair [25]. Alternative interaction configurations include creating "sleeves" within the composite laminates and various surface or edge attachment schemes [8, 25–27].

Advanced composites such as graphite/epoxy and glass/epoxy composites offer high strength and stiffness at a low weight and moderate cost, but they have poor resistance to impact damage because they lack an effective mechanism for dissipating impact strain energy such as plastic yielding in ductile metals. As a result, the composite materials dissipate relatively little energy during severe impact loading and fail in a catastrophic manner once stress exceeds the composite's ultimate strength. Typically, damage progresses from matrix cracking and delamination to fiber breakage and eventual material puncture [28–30]. Various approaches to increase the impact damage resistance and specifically, the perforation resistance, of the brittle composite materials have been examined. The popular design concept is to form a hybrid which utilizes the tougher fibers to increase the impact resistance and the stiffer and stronger graphite fibres to carry the majority of the load. The hybrids composed of the graphite/epoxy with Kevlar®, Spectra® and S-glass fibres have demonstrated modest improvements in impact resistance [28–30]. Amongst various engineering materials, high-strain SMAs have a relatively high ultimate strength and can absorb and dissipate a large amount of strain energy first through the stress-induced martensitic transformation and then through plastic yielding, as shown in Fig. 5. Accordingly, the impact resistance of the graphite/epoxy composites may be improved by hybridizing them with SMA fibres. Paine and Rogers

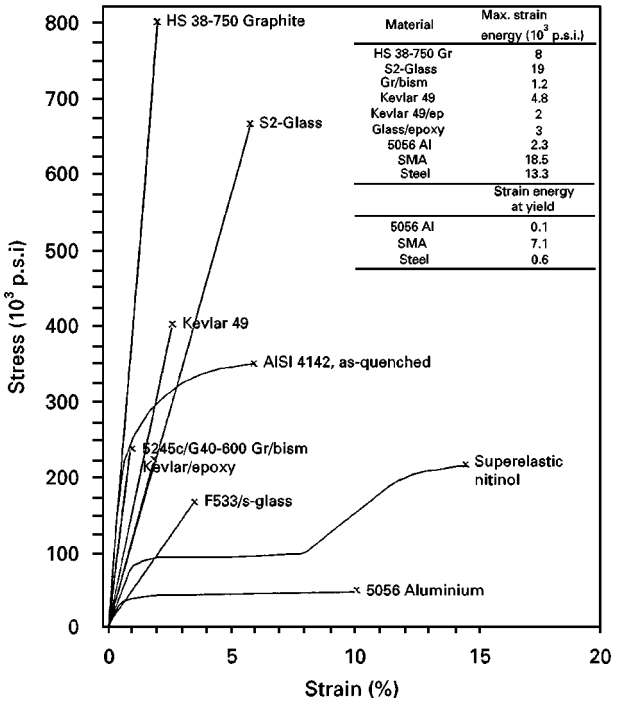

Material	Max. strain energy (10^3 p.s.i.)
HS 38-750 Gr	8
S2-Glass	19
Gr/bism	1.2
Kevlar 49	4.8
Kevlar 49/ep	2
Glass/epoxy	3
5056 Al	2.3
SMA	18.5
Steel	13.3

	Strain energy at yield
5056 Al	0.1
SMA	7.1
Steel	0.6

Figure 5 Stress–strain curves of various engineering materials [29]. The maximum strain energies for the materials are listed.

[8, 28] have developed the concept and demonstrated that under certain load conditions the impact energy absorbing ability of graphite and glass composites can be effectively improved by hybridizing the composites with Ti–Ni SMA fibres. Hybrid composites with improved impact and puncture resistance are very attractive because of their great potential in military and commercial civil applications.

2.2.2. Materials fabrication and characterization

The fabrication of hybrid composites with SMA fibres in polymer matrices has been addressed by many investigators [31–39]. Generally, the shape-memory hybrid composite materials can be manufactured with conventional polymer matrix composite fabrication methods, by laying the SMA fibres into the host composite prepreg between or merging with the reinforcing wires and then using either hot-pressing or an autoclave and several different types of cure cycles. Previously, a few attempts to incorporate embedded Ti–Ni wires directly into a polymer matrix composite proved largely unsuccesful due to manufacturing difficulties and problems associated with interfacial bonding [32]. To avoid the interfacial bonding issue, SMA wires were alternatively incorporated into polymer matrix by using coupling sleeves [25–27]. Both thermoset and thermoplastic composites have been addressed [28–39]. Comparatively, fibre-reinforced thermoplastics offer some substantial advantages over fibre-reinforced thermosets because of their excellent specific stiffness, high fracture toughness, low moisture absorption and possible fast and cost-effective manufacturing processes. However, the high processing temperatures may be problematic with respect to the embedding of SMA elements. The thermoplastic processing must be performed at higher temperatures, typically, between 423 and 673 K, whereas, the thermoset processing cycle of the composites is in the relatively low temperature range of RT–443 K. The thermoplastic processing cycle has some effect on the microstructure of the SMA fibres as manifested in the change in transformation temperatures and peak recovery stress: the transformation temperatures of the SMA shift upwards while the peak recovery stress drops as a result of the thermoplastic processing [31]. The thermoset processing only mildly affects the transformation characteristics of SMA fibres. However, some dynamical properties of SMA fibres may be significantly affected [39, 40].

Much of the previous research on the SMA hybrid composites utilized the one-way shape-memory effect, especially in the applications which require recovery stress of the SMA. Much care should be taken to prevent shape recovery of the prestrained SMA fibres or wires during the composite cure cycle. The complexity of manufacturing the SMA composites can be greatly simplified by using the two-way shape-memory effect [32, 34]. That is, the SMA wires will be trained to exhibit the two-way shape-memory effect prior to embedding in the matrix. The effect of processing parameters and training of the SMA elements on the performance of the SMA hybrid composites has been addressed by Paine and Rogers [31], White *et al.* [32, 33], and many other researchers [37, 38, 40].

Void content is one of the pressing issues in manufacturing the SMA hybrid composites. Voids in composite materials significantly affect the material integrity and behaviour. Their presence in the SMA composites will not only lead to property degradation of the host composite material, but the efficiency of activation and the level of interfacial bonding between the SMA fibres and host matrix will also be sacrificed. Accordingly, the void growth in the composites has been examined by White *et al.* [32, 34]. In the hot-pressed composites with graphite/epoxy laminates and embedded Ti–Ni fibres, the average void content was found to be 10.20%. Voids were shown to be concentrated near the embedded Ti–Ni wire locations. Additionally, the interfacial bonding was quite poor. The void content can be reduced to as low as 1.29% by autoclave stage curing [32].

Another issue of particular concern is the interfacial bonding. In the SMA hybrid composites, maximum interfacial adhesion between the SMA wire and the polymer matrix is desirable because most applications require maximum load transfer, and a strong interfacial bond also increases the structural integrity of the final composites [35, 41]. To improve the interfacial bonding, various surface treatments of the SMA fibres or introduction of a coupling interphase have been examined. Paine and Rogers [35] and Jonnalagadda *et al.* [36, 41] have estimated the interfacial bond strength of SMA fibres which were subjected to different surface treatments before embedding in various host polymer matrix composites. The pull-out test was used qualitatively to compare the interfacial adhesion. Five kinds of Ti–Ni fibres, that is, untreated,

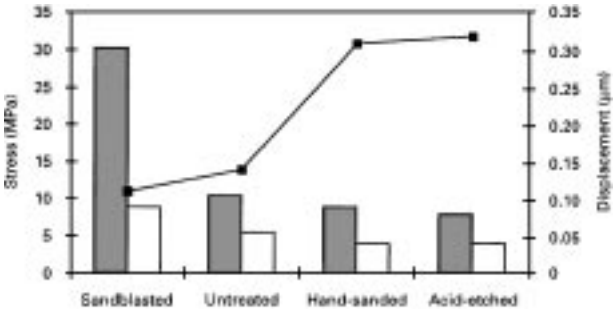

Figure 6 (■) Average interfacial debond strength, (□) maximum shear stress induced in the matrix, and (–■–) maximum displacement of embedded SMA wire, for the different surface treatment cases. Data source [41].

nitric acid-etched, hand-sanded, sand-blasted and plasma-coated, and two kinds of host matrix materials, i.e. graphite/epoxy and PEEK/carbon (APC-2) composites, were examined. The pull-out test results indicated that in the Ti–Ni fibres APC-2 system, a brittle interface failure without friction occurred, resulting in overall lower peak pull-out stress levels. In the Ti–Ni fibre/GR/EP system, however, a strong mechanical interaction or friction between the Ti–Ni fibre and GR/EP composite was involved. As a result, the fibre pull-out stress levels show a dependence on the adhesion between Ti–Ni fibres and host composite and, on average, the peak pull-out stresses are significantly higher than those in the APC-2 composites [35]. Generally, sand-blasting of Ti–Ni fibres increases the bond strength while handsanding and acid cleaning actually decrease the bond strength. Surprisingly, it was found that plasma coating of the fibres did not significantly alter the adhesive strength at all [35, 36, 41]. Jonnalagadda *et al.* [41] also measured the *in situ* displacements of embedded SMA wires and the resulting stresses induced in the matrix by using heterodyne interferometry and photoelasticity, respectively. As expected, the constraining effect of the matrix increases with increasing bond strength, causing a decrease in the displacement of SMA wire and a corresponding increase in the interfacial shear stress induced in the matrix, as illustrated in Fig. 6.

2.2.3. Modal modification and dynamic property tuning

2.2.3.1. Active and passive vibration control. Within the Rayleigh-Ritz approximation, the first natural frequency of the transverse vibration wave for a clamped SMA hybrid composite beam can be simply expressed as [42]

$$\bar{\omega}_1 = \frac{a}{l^2}\left(\frac{El}{\rho}\right)^{1/2}\left(1 - \frac{al^3}{8El}\right)^{1/2} \quad (3)$$

where a is a constant, ρ the density of the beam, l the length, El the bending stiffness, and q is the recovery stress generated by SMA fibres. The frequencies and the amplitues of the lower vibration modes are also functions of the recovery stress and stiffness [42–44]. Accordingly, the natural frequencies and vibration amplitudes of the composite beam can be altered by tuning the recovery stress of the embedded SMA fibres through heating. Bidaux *et al.* [39, 40] investigated the dynamic mechanical properties and phase transformation in polymer(epoxy)-based SMA composites with embedded Ti–Ni fibres. Although the martensites are constrained by the surrounding matrix, the onset and the evolution of the R-phase and martensitic transformation are only slightly affected by the presence of the matrix, but the dynamic moduli and the damping are significantly modified: in the composite with 1 vol% Ti–Ni fibres and prestrain of 5%, high forces and frequency changes up to 50% were observed, and the change in the resonance frequency is directly related to the change in the axial force. Heating the composite to temperatures close to the glass–rubber transition of the matrix may lead to large, irreversible changes of the vibration frequency. It should be noticed that the R-phase transformation in some Ti–Ni fibres may be more appropriate than martensitic transformation for applications in composites. This is because R-phase transformation exhibits a very high stress-rate that can give rise to large frequency changes per unit temperature (i.e. minimum electrical power). Meanwhile, because the transformation strain associated with the R-phase transformation is small, it is desirable for the composites to limit the shear stresses at the fibre–matrix interface which may lead to debonding. In addition, R-phase transformation exhibits a quite small transformation hysteresis, thereby making it feasible to control the properties precisely [40]. Unfortunately, R-phase transformation can be found only in some Ti–Ni-based SMAs with certain composition and usually after specific thermomechanical treatments.

Rogers [7] measured the natural frequency as a function of temperature for the graphite–epoxy beams with and without embedded SMA fibres. By embedding 15 vol% fraction of Ti–Ni fibres, the activated first frequency of the clamped–clamped beams at 422 K can be changed by as much as 520%, as shown in Fig. 7. For the SMA hybrid composites, it is more effective to control the vibration by activating the SMA fibres. Rogers *et al.* [24, 45, 46] calculated the first ten natural frequencies of the inactivated and fully activated composite plate and, the frequencies

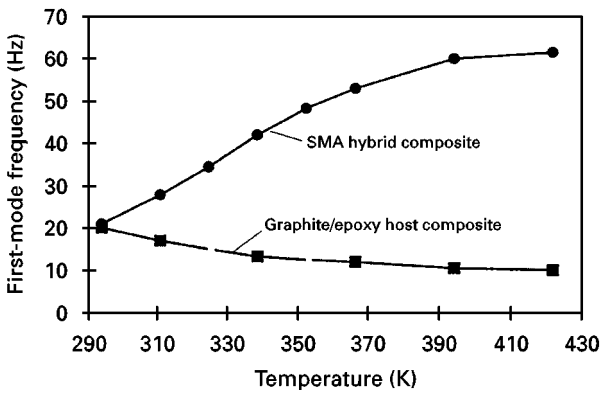

Figure 7 The first-mode frequency as a function of temperature for plain graphite/epoxy composite and the SMA hybrid [7].

were predicted to shift upwards with different levels, as shown in Fig. 8a. Schetky *et al.* [47] measured a total of 10 frequency response functions and 48 mode shapes for three kinds of boundary conditions, namely, clamped and simply supported, clamped–free, and clamped–free and partially activated. In all the cases, the resonant frequencies and the mode shapes were significantly altered by activating the SMA fibres. On average, however, the variations of the partially activated plate were greater than those achieved with the other two boundary conditions, as illustrated in Fig. 8b. This result suggests that partial activation of the composite plate spatially may lead to a greater efficiency in the vibration and acoustic control [45, 47]. Along with the changes in the first ten mode frequencies, varying degrees of decrease in the vibration amplitudes can be achieved [7, 24, 26, 42, 43].

The overall characteristics of the SMA hybrid composite are affected mainly through the edge-effect. A finite element analysis showed that as long as the SMA fibres are fixed, they may be embedded only around the composite plate edges and still provide the same control authority as SMA fibres embedded throughout the composite plate [48]. Extensive modal test results have confirmed the active modal modification capability of the composite structure [47]. Baz *et al.* [26] embedded SMA wires near the outer surfaces of rotating drive shafts to control the bending

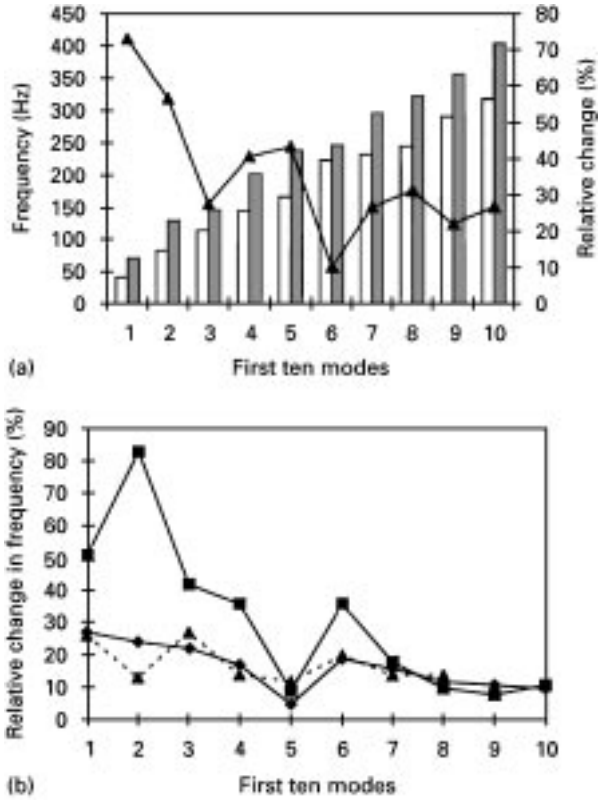

Figure 8 Effect of the SMA fibre activation and boundary conditions of the SMA hybrid composite beam on the changes in first ten mode frequencies. (a) Calculated results for (▮) activated and (▯) inactivated cases, and (▲) the change [46]; (b) experimental results for various boundary conditions, (▲) clamped–free, (■) partially activated, (-▲-) clamped–simply supported [47].

stiffness of the rotating beam. They observed changes in vibration amplitude of the beam and shafts and in the natural frequency of the first mode during activation of embedded Ti–Ni wires. They also inserted SMA wires with sleeves into flexible beams to control their buckling and vibration behaviour and they showed that the buckling load of a flexible fibreglass composite beam can be increased by a factor of three as compared to the buckling load of an uncontrolled beam [26, 33]. Epps and Chandra [27, 49] also demonstrated the active-tuning capacity of graphite–epoxy rectangular solid section beams with SMA wires inserted in embedded sleeves. The SMA wires were activated using electrical resistance heating, and a large tensile strength recovery force developed in them due to the mechanical constraints provided by the clamps at both ends of the beam. The recovery stress was predicted using a finite element constitutive model and compared well with experimental results. A 22% increase in the first natural frequency was shown by using 2% volume fraction of SMA wires, and a 23% increase in the fundamental frequency of an actual helicopter composite shaft with 7.4% volume fraction of SMA wires embedded was demonstrated [49].

From the standpoint of passive vibration control, high inherent material damping is desirable for adaptive composite structures because it can be effectively tailored to enhance the overall passive damping of structural dynamic systems. The damping capacity of SMA smart composite laminae have been evaluated through analytical integrated micro-macro-mechanical approaches by Baburaj and Matsuzaki [50, 51]. In their approach, two different types of matrices, namely, intermediate-modulus high-strength (IMHS) DX210 epoxy and intermediate modulus low-strength (IMLS) polyester were considered; and the Ti–Ni fibres were assumed to be embedded in three kinds of primary host materials, namely, E-glass fibres with DX210 epoxy(E-glass/IMHS), high-modulus surface-treated graphite fibres with DX210 epoxy (HMS/IMHS) and with polyester (HM-S/IMHS). It was found that the factors such as SMA fibre volume fraction, the fibre orientation and the stacking sequence of SMA composites have strong influences on the specific damping capacity (SDC) and on the natural frequencies of the SMA hybrid composites and structures [50]. A considerable enhancement of the modal SDC was observed as the SMA fibre volume fraction increases in the host material. For example, as much as 35% enhancement of longitudinal SDC could be achieved by embedding 5 vol% Ti–Ni fibres to a conventional HM-S/IMHS composite, while a 17% enhancement of modal SDC in the fundamental mode was possibly by 10% increment of Ti–Ni fibre in the E-glass/IMHS host material. In both the cases, the volume fraction of matrix material was kept at 50%. The modal SDC of the first three modes were found to decrease gradually as the SMA fibre orientation increases, with a maximum when the laminate angle is 0° and a minimum at $\pm 45^\circ$. Meanwhile, in all cases, the natural frequencies change in an opposite way to the modal SDC [51].

2.2.3.2. Acoustic radiation and transmission control. In addition to the natural frequencies, the mode shapes of the SMA composite structures are changed or modified by activating the embedded SMA fibres [24, 45–47]. The variations and modifications of natural frequencies and the mode shapes have a significant impact on the control of structural acoustic radiation and transmission. Based on the numerical analyses in terms of composite modes instead of the usual characteristic modes, Liang *et al.* [46] investigated the directivity pattern, acoustic transmission loss and radiation efficiency of SMA hybrid composite plates (Ti–Ni/graphite/epoxy laminae, with 10 vol % Ti–Ni fibres) for the activated and inactivated cases, using both APT and ASET control strategies. An examination of the results revealed the following features.

1. The directivity pattern is governed mostly by the composite mode of the plate and, as the frequencies increase, more transmitted sound becomes concentrated at the transmitted angle which is close to the sound incident angle. Moreover, the directivity pattern at high frequencies where the modal density is increased might not be changed very much by activating the SMA fibres, instead, the magnitude of the transmitted power can be changed significantly in such cases.
2. For the inactivated plate, at low frequencies the radiation efficiencies of the fourth, sixth and seventh modes are higher than those of the second and third modes while the first mode is the most efficient radiator. When activated, the first mode remains largely unchanged, but the order of the second and third mode is changed by shifting their relative position, and the tenth mode is also changed significantly. The dominating modes of the plate response at different excitation frequencies depend on the transmission power of the individual modes and their coupling effects. For instance, at 220 Hz excitation frequency, the sixth and seventh rather than the first and second are the dominating modes.
3. The main effect of activation of the embedded SMA fibres is to shift the dip in the transmission loss profile to higher frequencies, whereas the transmission loss is reduced in an average sense over the frequency range examined [46]. Accordingly, it is feasible to implement the structural acoustic control algorithm by activating the SMA fibres to disturb the dominating mode shapes and shift the natural frequencies away from the frequencies that most efficiently transmit the sound.

Experimental investigations have demonstrated the feasibility of utilizing the SMA-reinforced composites to allow minimization of radiated sound for harmonic beam vibration and placement of peak radiation response at specified frequencies within a controllable range [52]. Measurements of the sound radiation from clamped–baffled TiNi-reinforced graphite–epoxy composite beams were performed using two different control strategies, namely, minimization control and frequency placement control. The closed-loop minimization control algorithm was aimed to shift beam resonances away from discrete, harmonic, disturbance frequencies, minimizing the acoustic radiation. Various disturbance frequencies were selected to coincide with beam-resonant frequencies of the SMA composite beam and in all the cases the sound pressure was effectively reduced to the background noise levels. For a sinusoidal disturbance at 32 Hz (=first mode), controlled sound pressure levels showed a reduction of 20–25 dB. For excitation at 145 Hz (=fourth mode), the sound reductions were about 25–30 dB. The peak radiation frequency placement control, using a thermal model based on the correlations between the frequencies of the lower order vibration modes and the composite beam bulk temperature, allowed tuning of the beam radiation response anywhere within an octave bandwidth above the fundamental mode [52]. Active modal modification in conjunction with active strain-energy tuning has been shown to be effective in reducing sound transmission response [8]. These results indicated that a SMA composite structure may be tailored to give a uniform dynamic response over a large temperature range or give some other adaptive dynamic response as a function of temperature.

2.2.4. Active structural modification

Deflection and shape control can be accomplished using the same techniques as described for vibration control tasks. However, differing from applications where only stress-stiffening is required, active shape control requires a combination of high recovery forces and recovery strains from the SMA elements to produce significant shape change in the host structure. Accordingly, either large SMA volume fractions are necessary to cause quickly significant levels of shape change in graphite- and glass-reinforced composite structures or, the shape change occurs only at quasi-static rates [8, 24]. Active buckling control can be imagined in which SMA fibres are stiffened within a composite to alter the critical buckling load of the structure. However, depending on the boundary conditions and orientation of the embedded SMA fibres, the critical buckling load may be either increased or decreased by changing the Young's modulus of the SMA fibres and by introducing distributed in-plane loads to the structure [24]. Chaudhry and Rogers [53, 54] have numerically analysed the deflection and buckling of a laminated composite plate with embedded SMA fibres. Using active strain-energy tuning and active property tuning techniques, the maximum deflection for several activation schemes was demonstrated. Baz *et al.* [26, 55] have shown that discrete Ti–Ni SMA actuators can be used to control buckling of flexible composite beams. In the composite beams, the SMA strips were embedded inside sleeves which were located at the neutral planes and arranged parallel to the longitudinal axes of these composite beams. The results indicated that by incorporating SMA elements in the structure it would be feasible to control the shape of composite beams without compromising their structural stiffness or frequencies. Lagoudas and co-workers [56, 57] have developed the theory on the deformation of flexible rods with various configurations of embedded SMA wires. The deformed shapes

and extent of deflection for various SMA wire configurations were determined and the thermal response of the active flexible rods was also evaluated. Pfaeffle *et al.* [58] presented some experimental results on the rods with prestrained SMA wires which were embedded off-axis in elastomeric cylinders. The effects of some parameters such as SMA/rod interfacial shear strength and number of SMA wires for creating optimal shape control in the flexible rods were investigated and some design strategies for rod fabrication were suggested. Shahinpoor and Wand [59, 60] designed and modelled the novel fibrous SMA "muscle". Numerical approaches using finite element method predicted that a large deflection of the bending muscle, which was composed of a flexible beam, a thin-wall elastic tube, and an embedded Ti–Ni SMA wire as an actuator, could be realized under small change of strain in the SMA wire. More structural modification approaches utilizing SMA fibres can be found elsewhere [60–64].

Bi-directional environmentally responsive composites composed of Ti–Ni fibres and carbon fibre-reinforced thermoplastic were designed by Yoshida *et al.* [65, 66]. Although the response and recovery rate need further improvements, superior performance and responsive shape control of the composite could be achieved by the appropriate choice of properties, geometries and volume fractions of the SMA elements and the matrix. Because the SMA elements are usually activated by resistive heating, the response time is ultimately limited by the cooling process. The usable bandwidth of SMA actuators for structural control can be increased by using several actuators in parallel and energizing subsets of these during successive cycles of structural motion. Tests showed that both the first and second modes of a Ti–Ni composite cantilevered beam could be excited through sequential excitation of the SMA wires [67].

In some static or quasi-static structural control applications, the deflection should be minimized and must return to its original shape after being deformed by a load. In design of composite pressure vessels, multi-layer composite cylinders are preferable to thick-wall, single-layer cylinders because the inner layers can expand and transfer load to the outer layers, allowing the entire wall thickness to be loaded as efficiently as possible with no problematic residual stress. Polymer matrix composite (PMC) cylinders expand or dilate under internal pressure much more than their equivalent metallic counterparts for their lower transverse and wire direction elastic moduli, but the excessive radial expansion of the multi-layer designs may limit their use in applications requiring metallic liners or internal pistons without leakage [68]. Accordingly, the radial dilation should be as small as possible. Paine and Rogers [68, 69] designed an adaptive SMA composite cylinder to reduce the radial expansion. The SMA wire rovings were impregnated with polymer resins to form a shape-memory alloy composite (SMAC) or Ti–Ni/epoxy composite. The composite was wrapped as a separate layer around or within other PMC cylinder layers, much like filament winding of the composite-reinforcing fibres. The prestrained SMA wires generate a controllable level of recovery stress when activated. Consequently, the recovery stress produces an active external pressure against the inner PMC layer, producing a compound cylinder effect that can be used to reduce radial expansion and some of its harmful effects. Theoretical modelling of graphite/epoxy, glass/epoxy, and Kevlar®/epoxy composites predicted that the SMAC outer layers generate preferential compressive stresses in the inner composite layers and hence reduce the peak hoop stresses or increase the loading capacity. In a graphite/epoxy/SMA composite cylinder with a 55° ply angle lay-up, a reduction in peak tensile hoop stresses of 344.7 MPa (50×10^3 p.s.i.) was demonstrated [68]. Experimentally, a reduction of the radial expansion by 0.3% in glass/epoxy-SMAC composite cylinders was observed [69]. The SMA composite cylinders make it possible to produce composite cylinders with thinner walls than monolithic PMC designs and with significantly lower weight than monolithic metal. Because the SMAC-induced pressure can be turned on or off, the active composite cylinder will not cause binding of the cylinder wall with the internal piston when the cylinder is at lower pressures. However, local buckling of the inner composite layers may be a problem in the case of passive SMA composite cylinders design.

For smart structural applications involving actuation, such as buckling and shape control, the durability of the hybrid composite should be given a due consideration. Friend *et al.* [70–72] and Doran [73] have addressed this issue with unidirectional glass fibre-reinforced epoxy laminates containing Ti–Ni SMA fibres orientated parallel to the glass-fibre direction. The maximum deflection of the composite cantilever beam increases with increasing prestrain and volume fraction of SMA fibres. However, degradations or instabilities in both inactivated shape and activated deflection response were observed during cyclic actuation of the hybrid composite. In particular, a dramatic decrease in output strain was observed during the first cycle of actuation. Initially, Friend and Morgan [70, 71] ascribed the instabilities to the accumulation of internal damage resulting from interfacial decohesion and thermal degradation. Later, they suggested that the degradation originated from the effect of initial manufacturing and operating conditions on the SMA performance [72]. The level of the degradation is controlled by the prestrain, the inherent elastic stiffness of the composite beam, and the volume fraction of the SMA fibres [73].

2.2.5. Impact damage resistance

As shown in Fig. 5, shape-memory alloys dissipate the strain energy of the order of four times of high alloy steel and 16 times that of many graphite/epoxy composites through the stress-induced martensitic transformations. The unique strain energy absorbing capacity of SMAs can be used to actively control the propagation of cracks. Rogers *et al.* [74] proposed a method to use shape-memory alloys as actuators in order to extend material life-span by accelerating

closure of fatigue cracks and lowering crack propagation speed using multiple shape-memory alloys fixed at the bottom of the notch part where stress concentration took place and by applying electric currents there to raise temperature, thus causing contraction forces and lowering the average stress at the point. Du and Nie [75] showed that stress concentration at notch tips can be reduced by placing prestrained Ti–Ni wires on the surface of tensile test specimens made of epoxy resin and by applying electric heating to the Ti–Ni wires to make them contract with shape memory.

Of particular interest, however, are the recent attempts made by Paine and Ellis *et al.* [28–30, 76–81] to improve the impact damage resistance of brittle thermoset matrix composite materials by hybridizing the composites with SMAs. The response of various SMA hybrid composites with different interaction configurations to low, high and ballistic velocity impact were examined.

2.2.5.1 Low-velocity impact. Ti–Ni fibre/epoxy composite materials with fibre volume fractions of the order of 10–25% were laminated to host composites as surface layers instead of being embedded, to facilitate observation of the failure modes and simplify fabrication. Two types of host composites were used: graphite/bismaleimide (gr/bis) and glass/epoxy (gl/ep). An aluminium/epoxy composite and Kevlar/epoxy composite were also used as comparison hybrid layers. The low-velocity impact test (velocity $<6\,m^{-1}s$) was performed using an instrumented drop-weight impact tester; the dissipated impact energy and deflection during impact were determined from force–time data [28, 30, 76, 77]. The ability of various materials to resist the motion of the tup during low-velocity perforation can be illustrated from the load versus displacement response. The results are summarized in Fig. 9(a). The normalized energy values represent the amount of energy per unit volume required to perforate the various materials. It is evident that the Ti–Ni/graphite composite produces an increase of 35% for the volume-normalized perforation energy over the monolithic gr/ep host composite, whereas the aluminium and Kevlar hybrids produce little or no increase at all in the energy. For the glass/epoxy system, because the monolithic gl/ep composite demonstrated significantly greater impact toughness than the monolithic gr/ep composite, the affect on the perforation energy was not so pronounced. The SMA hybrids demonstrated a slightly improved perforation toughness whereas the aluminium and Kevlar® hybrid composites showed a diminished benefit. Visual inspection revealed that the composite with SMA fibres resisted the cutting action through distributing the impact load over a greater surface area, because SMA remained intact during the perforation event. The monolithic gr/ep and gl/ep, and the aluminium and Kevlar® hybrids all failed locally from a punched or cut hole from the local transverse shear stresses at the edge of the impact site [28, 30].

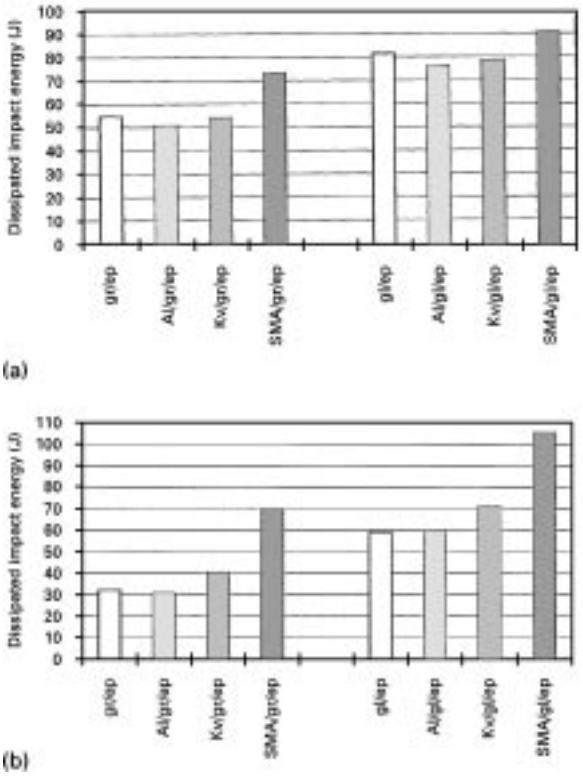

Figure 9 Comparison of the impact energy absorption for various composites under (a) low-velocity impact test and (b) high-velocity impact test. Data source [28]. The dissipated energies are volume normalized.

The low-velocity impact experiments on graphite/bismaleimide composite laminates with 2.8 volt % embedded SMA fibres were also performed by Paine and Rogers [76]. The tests on both clamped "large deflection" and clamped–clamped "small deflection" specimens revealed that the impact resistance could be greatly improved by embedding SMA fibres, as shown by the remarkable increase in the peak impact force and the reduction of the impact-induced delamination area by as much as 25% [76]. More recently, Kiesling *et al.* [29] investigated thin graphite/bismaleimide composites embedded unidirectionally and bi-directionally with 3 and 6 vol % Ti–Ni fibres, respectively. The results showed that while the stiffness and ultimate strength of the composite remained unchanged, an increase in absorbed impact energy of 41% was observed in bi-directional SMA hybrids and 23% in unidirectional SMA hybrids. However, C-scans of the bi-directional SMA hybrids showed a 22% larger delamination area as compared to plain gr/ep composite [29]. A quasi-static model [79] demonstrates that contact deformation, global bending deformation and transverse shear deformation are the energy absorption mechanisms for the SMA/graphite/epoxy composites under a low-velocity impact. At very low velocities, the contact energy absorption is the most effective mechanism, while the shear deformation absorbs most of the impact energy at higher impact velocities. The total energy absorption of the SMA hybrid composites increases when the stress-induced martensitic transformation occurs. These results shed some light on the design of the

SMA hybrid composites with improved impact-damage resistance.

2.2.5.2. High- and ballistic-velocity impact. Usually, high-velocity impact refers to such situations as a bird colliding with an airplane at the speeds in the range of 30.48–243.84 m s^{-1} (100–800 ft s^{-1}), while ballistic impact events include situations such as a projectile fired from a gun at speeds exceeding 243.84 ms^{-1} (800 ft s^{-1}) [78]. Because the high- and ballistic-velocity impact events are characterized by a much more local response of the composite than the low-velocity impact events, the impact results may demonstrate significantly different behaviour from the low-velocity test. Paine and Rogers [28] performed the high-velocity impact test at a velocity of up to 152.40 m s^{-1} (500 ft s^{-1}) by using a non-instrumented gas gun. The impact energies of surface-layered SMA hybrid composites were determined from impact velocity. The perforation energy values normalized by volume are presented in Fig. 9b. As shown in the figure, for the graphite/epoxy system, the SMA hybrid composite increased the perforation toughness by 100%, and for the glass/epoxy system an increase of 67% was demonstrated. In both the systems, the Kevlar® hybrid composites demonstrated only a slight improvement to impact energy, while the aluminium hybrid showed little, if any, improvement.

Ellis *et al.* [78, 80] investigated the ballistic-impact resistance of the graphite composites with various SMA component configurations by using a 9 mm Beretta handgun with the projectile velocity greater than 274.32 m s^{-1} (900 ft s^{-1}). The unidirectional Ti–Ni SMA fibre layer with 1.2 vol% was embedded on the front face, in the middle, and on the backface of the host graphite/bismaleimide composite, respectively, to form three hybrid configurations. The impact results revealed that the backface appeared to be the most suitable location of the SMA fibres in the hybrid composite, and no increase in the energy absorption was observed when the SMA fibres were placed on the front and middle locations. In all cases, the SMA fibres were typically pulled through the graphite without being strained to their full potential, resulting in a slight, if any, improvement in the high-velocity impact resistance. Increasing the volume fraction of the unidirectional SMA fibres or adding two perpendicular layers of SMA fibres on the backface of the composite yielded no remarkable increase in energy absorption. These facts suggest that the high strain-energy absorption capabilities of SMA were not fully utilized at ballistic velocities because of the high strain-rate effects coupled with a strain mismatch between the relatively tough SMA fibres and the brittle cured epoxy resin [78]. However, the SMA fibres were found to be more effectively used when embedded between layers of the thermoplastic extended-chain-polyethylene (ECPE, or Spectra™) prepreg which were then placed on the backface of the graphite composite: an increase of 23–24% in the energy absorption was achieved when compared to the plain graphite composite. Nevertheless, the SMA fibres were still not fully utilized as evinced by the lack of fibres strained to failure [80] ; more work is needed in this area.

The SMA hybrid composites with improved penetration resistance may be useful in both military and civil applications, such as helmets, portable lightweight shelters and other personal armour systems for ballistic protection [28, 29, 80].

2.3. Shape-memory polymer hybrid composite laminates

Advanced composite laminates such as carbon fibre-reinforced plastics (CFRP) have a relatively low damping capacity, that can be improved by hybridizing CFRP with aramid or glass fibre-reinforced plastics (GFRP), or adding other polymeric damping materials to them. The latter approach has been proved to be more effective than the former [81]. Because shape-memory polymers (SMPs) have a high-damping capacity, and the glass transition temperature, T_g, where the loss factor $\tan\delta$ reaches a maximum value, can be easily controlled, they can be utilized to improve the damping capacity of the laminates. Accordingly, Fukuda *et al.* [81] designed an SMP hybrid composite by sandwiching the shape-memory polymer between layers of CFRP or GERP composite laminates. Three kinds of shape-memory polymer films, named by SMP-L, SMP-M and SMP-H, having approximately the same maximum value of loss tangents (maximum $\tan\delta = 1.0$) at 299, 334 and 365 K, respectively, were prepared. The interleaved composite laminates integrating an SMP film about 100 μm thick between four plies of CFRP and GFRP prepreg sheets were cured in a hydraulic press. The SMP/CFRP composite with a thickness of about 2 mm and the SMP/GERP composite with a thickness of about 1.5 mm were cured at 393 and 443 K for 4 h, respectively. The loss tangents were measured at a frequency of 1 Hz in the temperature range from 283–393 K. It was found that the $\tan\delta$ of CFRP and GERP was significantly improved near the T_g of each SMP. The amount of improvement for CFRP was superior to that for GFRP: the maximum $\tan\delta$ for SMP/CFRP composite was about 400 times that of CFRP, and only 30 times in the case of GFRP. Experimental results of the maximum loss tangents and the corresponding peak temperatures, T_p, for the SMP and their hybrid laminates are summarized in Table I. In addition, it was found that within the frequency range 0.1–10 Hz, the change in frequency had no remarkable effects on the $\tan\delta$ of the laminates. Tensile tests results indicated that the tensile strength and modulus of SMP/GFRP laminates were almost the same as those of GFRP, but in the case of CFRP, a reduction of about 15% in the strength and modulus was observed [81].

Shape-memory polymers may also serve as the host matrix material to form adaptive composites. Liang *et al.* [82] used various kinds of fibres such as chopped fibreglass, unidirectional Kevlar® fibre and woven fibreglass in SMP melts to fabricate fibre-reinforced thermoplastic composites by using a hot press. It was

TABLE I Summary of experimental data on maximum loss tangent for SMP, CFRP and GFRP composite laminates [81]

Material	Maximum $\tan\delta$	Peak temperature T_p(K)
SMP-L	1.0	299
SMP-M	1.0	334
SMP-H	1.0	365
CFRP	3.5×10^{-4}	–
CFRP/SMP-L	1.1×10^{-1}	309
CFRP/SMP-M	1.4×10^{-1}	340
CFRP/SMP-H	1.5×10^{-1}	365
GFRP	6.0×10^{-3}	–
GFRP/SMP-L	2.3×10^{-1}	320
GFRP/SMP-M	1.8×10^{-1}	349
GFRP/SMP-H	2.6×10^{-1}	362

shown that in the as-fabricated SMP composites there is a good bonding between the fibres and the SMP matrix. Tensile tests indicated that the fibre-reinforced SMP composites had improved strength and modulus over monolithic SMP. The woven fibreglass SMP composite had the highest ultimate strength and Young's modulus. Its strength increased by 50% and its modulus by almost four times. In addition, the chopped fibreglass-reinforced SMP composite had a higher elongation limit of 3% at 6.7% strain rate, in comparison with the value of 1.5% for woven fibreglass SMP composite. Because the Young's modulus of the embedded fibreglass is much greater than that of SMPs, the SMP composites did not exhibit shape-memory effect in the direction of the fibres. However, a certain amount of bending deflection recovery was observed in bending tests. It was found that the SMP solution was much more suitable to make composite prepregs than general fibre-reinforced thermoplastics. SMP laminates were hot-press fabricated from the SMP composite prepregs using Kevlar®, Spectra®, high-stiffness S-glass fibres and DMF(*N*,*N*-dimenthylformamide) SMP solution resin [82]. The characterization of the fabricated SMP composite laminates is, however, not often reported in the open literature.

3. Particulate-reinforced shape-memory composites

3.1. SMA particulate/aluminium matrix composites

3.1.1. Material design

Particulate-reinforced metal matrix composites (MMCs) have attracted considerable attention because of their feasibility for mass production, promising mechanical properties and potential high damping capacity. In applications not requiring extreme loading or thermal conditions, such as automotive components, the discontinuously reinforced MMCs have been shown to offer substantial improvements in mechanical properties. In particular, discontinuously reinforced aluminium alloy MMCs provide high damping and low density and allow undesirable mechanical vibration and wave propagation to be suppressed [83]. As in the fibre-reinforced composites, the strengthening of the composites is achieved through the introduction of compressive stresses by the reinforcing phases, due to the mismatch of the thermal expansion coefficient between the matrix and reinforcement. The most frequently used reinforcement materials are SiC, Al_2O_3 and graphite (Gr) particles. Although adding SiC and Al_2O_3 to the aluminium matrix can provide substantial gains in specific stiffness and strength, the resulting changes in damping capacity may be either positive or negative. Graphite particles may produce a remarkable increase in damping capacity, but at the expense of elastic modulus [83]. More recently, Yamada *et al.* [84] have proposed the concept of strengthening the aluminium MMCs by the shape-memory effect of dispersed Ti–Ni SMA particles. The strengthening mechanism is similar to that in the SMA fibre-reinforced composites: the prestrained SMA particles will try to recover the original shape upon the reverse transformation from martensite to parent (austenite) state by heating and hence will generate compressive stresses in the matrix along the prestrain direction, which in turn enhances the tensile properties of the composite at the austenitic stage. In the light of the well-known transformation toughening concept, some adaptive properties such as self-relaxation of internal stresses, can also be approached by incorporating SMA particles in some matrix materials. Because SMAs have a comparatively high loss factor value in the martensite phase state, an improvement in the damping capacity of the SMA particulate-reinforced composites is expected at the martensite stage. Accordingly, SMA particles may be used as stress or vibration wave absorbers in paints, joints, adhesives, polymer composites and building materials.

3.1.2. Materials preparation

Shape-memory particulate-reinforced composites can be fabricated by consolidating aluminium and SMA particulates or prealloyed powders via the powder metallurgical route. SMA particulates may be prepared with conventional processes such as the atomization method and spray or rapid solidification process that may produce powders with a size ranging from nanometres to micrometres. However, few reports on the production of SMA particles are recorded in the open literature. Recently, Cui [85] has developed a procedure to prepare Ti–Ni–Cu SMA particulates through hydrogenating–ball milling–dehydrogenating. The ternary Ti–Ni–Cu alloys, where there is a substitution of nickel by copper by up to 30 at %, are of particular interest for their narrow hysteresis, large transformation plasticity, high shock absorption capacity and basic shape-memory effect. Owing to their unique properties, the ternary Ti–Ni–Cu alloys have shown some promise as smart materials with actuation, sensing and adaptive strengthening characteristics [86]. When the content of copper exceeds 15 at %, the ternary alloys become very brittle and hence much more easily broken down into particulates by ball milling. Although it was reported

previously [87] that Cu–Zn–Al alloy powders had been prepared from commercial Cu–Zn and aluminium powders using the mechanical alloying technique, there was no physical evidence to prove that thermoelastic martensitic transformations occurred in the as-received powders. In fact, most of the attempts to prepare the Ti–Ni and copper-based SMA particulates by ball milling were unsuccessful, due to the complex mechanical alloying reactions and contaminations during the process [85].

In an exploratory attempt [88], a $Ti_{50}Ni_{25}Cu_{25}$ alloy was prepared in a high-frequency vacuum induction furnace. The ingot was homogenized at 1173 K for 10 h. The bulk specimens were cut from the ingot. Chips with a size of about 0.1 mm × 3 mm × 30 mm from the ingot were hydrogenated at 673 K for 5.8 h in a furnace under a hydrogen atmosphere, then the chips were ball milled in a conventional planetary ball mill, the weight ratio of balls to chips being 20:1. The vials were filled with ether and the rotational speed of the plate was kept constant during milling. The milled powders were then dehydrogenated in a vacuum furnace at 1073 K for 10 min at a vacuum of 10^{-3} Pa. The X-ray diffraction and transmission electron microscopy (TEM) observations indicated that the as-received Ti–Ni–Cu particulates, similar to the bulk counterpart, possessed a mixture structure of B19 and B19′ martensites. Differential scanning calorimetry (DSC) results demonstrated that the particulates exhibit excellent reversible martensitic transformations, though the peak temperatures were slightly altered when compared to the bulk material. The Ti–Ni–Cu/Al composite was prepared from 99.99% Al powders of size 2–3 μm and the Ti–Ni–Cu powders with a size of about 30 μm. The volume ratio of the Ti–Ni–Cu powder to aluminium powder was 3:7. The powders were mixed in a mixer rotated at 50 r.p.m. for 10 h. The consolidation of the mixed powders was achieved by hot isostatic pressing (HIP) at 793 K for 10 min, the relative density of the compact being 98.5%. Fig. 10 shows the scanning electron microscopy (SEM) morphology of the as-consolidated Ti–Ni–Cu/Al composite. The X-ray profile, as shown in Fig. 11, is clearly a combination of martensite and aluminium.

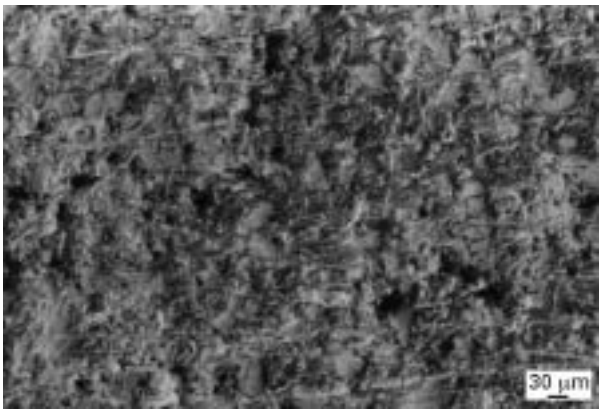

Figure 10 SEM morphology of the as-received TiNiCu/Al composite.

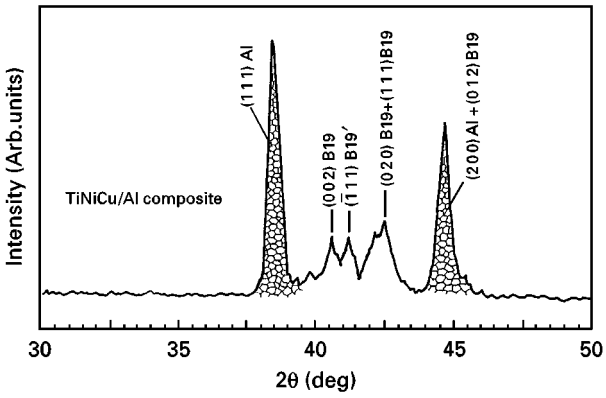

Figure 11 X-ray diffraction profile for the as-fabricated TiNiCu/Al composite.

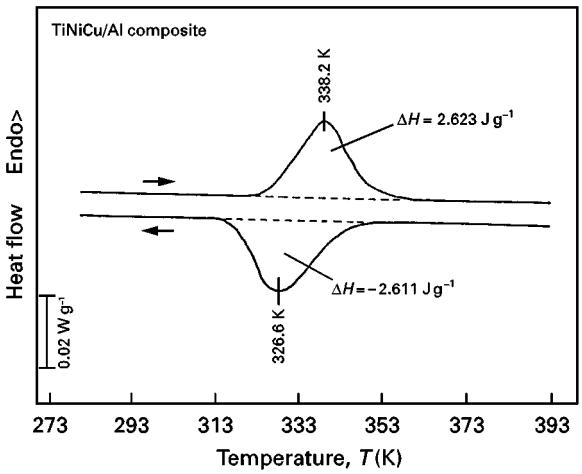

Figure 12 DSC heating and cooling curves showing the reversible martensitic transformation in the TiNiCu/Al composite.

3.1.3. Materials performance

The DSC measurements of the Ti–Ni–Cu/Al composite as shown in Fig. 12 are evidence of the occurrence of the thermoelastic martensitic transformations, just as demonstrated in the Ti–Ni–Cu bulk and particles. The reversible transformations could be repeated when the composite was thermally cycled between 273 and 423 K. These preliminary results clearly suggest that it is feasible to produce some adaptive characteristics within the composite through the shape-memory alloy particulates. Systematic investigations of the damping capacity and mechanical properties of the composite are under way.

Based on the Eshelby's equivalent inclusion model, Yamada *et al.* [84] have calculated the residual stress and stress–strain curve of the Ti–Ni dispersed aluminium matrix composites. The results predicted that the residual stress along the longitudinal direction is compressive and that along the transverse direction is tensile when the SMA particles are given tensile prestrain along the longitudinal direction. On the contrary, compressive and tensile residual stresses are induced in the transverse and longitudinal direction, respectively, when the particles are given compressive prestrain along the longitudinal direction. The level of

the residual stress increases with increasing prestrain and volume fraction of SMA particles. As a result, the yield stress of the composites shows a corresponding enhancement effect. It is predicted that the yield stress may be more than doubled when reinforced by only a few per cent volume fractions of SMA particles. Young's modulus of the composite is not affected by the prestrain but only by the volume fraction of the particles. The work-hardening rate also increases with the volume fraction of particles, but the amount of increase in the flow stress of the tensilely prestrained composite is larger than that of the compressively prestrained one [84].

In an attempt to design an adaptive solder joint, Trombert *et al.* [89] proposed the approach of incorporating Ti–Ni SMA particles in a SnPb solder paste to increase the yield stress and reduce the thermally induced stresses. Computer simulation results indicated that the mean equivalent stress in the composite solder joint can be substantially reduced [89].

3.2. Ceramic particulate/SMA matrix composites

In a shape-memory alloy matrix, dispersed second-phase particles may precipitate or form during solidification or thermal (mechanical) processing, thereby creating a native composite. The martensitic transformation characteristics and properties of the composites can be modified by control of the particles, as demonstrated in Ti–Ni(Nb), Cu–Zn–Al and Cu–Al–Ni–Mn–Ti alloys [90]. Alternatively, the presence of a ceramic second phase within the SMA matrix may lead to a new composite with decreased density and increased strength, stiffness, hardness and abrasion resistance. Compared with common ceramic/metal composites, a higher plasticity may be expected for this composite, because the stress-induced martensitic tranformation may relax the internal stress concentration and hence hinder cracking. Previously, Al_2O_3 particle-reinforced Cu–Zn–Al composites were prepared with conventional casting method, and this kind of composite was suggested to be suitable for applications requiring both high damping and good wear resistance [91]. Using explosive pressing of the powder mixture, a TiC/Ti–Ni composite was prepared [92, 93]. In the sintered TiC/Ti–Ni composite it was found that the bend strength, compression strength and stress intensity factors were significantly higher than those for TiC/Ni and WC/Co composites. With increasing TiC content, the hardness and compressive strength increase, while the ductility and toughness decrease [92, 93]. More recently, Dunand and co-workers [94–97] systematically investigated the Ti–Ni matrix composites containing 10 and 20 vol% equiaxed TiC particles, respectively. The composites were prepared from prealloyed Ti–Ni powders with an average size of 70 μm and TiC particles with an average size of about 40 μm, using powder metallurgy technique. The TiC particles modify the internal stress state in the Ti–Ni matrix and, consequently, the transformation behaviour of the composite: the B2-R transformation is inhibited; the characteristic temperatures A_s and M_f are lowered, while the M_s temperature remains unchanged; and the enthalpy of the martensitic transformation is reduced. Unlike composites with matrices deforming solely by slip, the alternative deformation mechanisms, namely, twinning and stress-induced transformation, are expected to be operative in the Ti–Ni composites during both the overall deformation of the matrix and its local deformation near the reinforcement, thereby resulting in the pseudo-elasticity and rubber-like effect. Compared to unreinforced Ti–Ni, the range of stress for the formation of martensite in the austenitic matrix composite is increased and the maximum fraction of the martensite is lowered. For both the austenitic and martensitic matrix, a strengthening effect can be observed: the transformation or twinning yield stress is increased in the presence of the dispersed TiC particles. However, for the austenitic matrix, the transformation yield stress is higher than that predicted by Eshelby's load-transfer theory, due to the dislocations created by the relaxation of the mismatch between matrix and particles. In contrast, for the martensitic matrix, the twinning yield stress and the apparent elastic modulus are less than those predicted by Eshelby's model because of the twinning relaxation of the elastic mismatch between matrix and reinforcement. Besides the elastic load transfer, the thermal, transformation, and plastic mismatches resulting from the TiC particles are efficiently relaxed mainly by localized matrix twinning, as revealed by neutron diffraction measurements. As a result, the shape-memory capacity, that is, the extent of strain recovery due to detwinning upon unloading, is scarcely affected by the presence of up to 20 vol% ceramic particles [94–97].

3.3. Magnetic particulate/SMA matrix composites

Giant magnetostrictive materials $(Tb_yDy_{1-y})_xFe_{1-x}$ (Terfenol-D) provide larger displacements and output energy density, and superior manufacturing capabilities, as compared to ferroelectrics. However, their applications have been limited by the poor fracture toughness, eddy current losses at higher frequencies, and bias and prestress requirements. More recently, composite materials based on Terfenol-D powders and insulating binders have been developed in Sweden [98, 99]. These composites broaden the useful range of the Terfenol-D material, with improved tensile strength and fracture toughness, and the potential for greater magnetostriction and coupling factor. Most recently, Ullakko *et al.* [100, 101] proposed a design concept to embed Terfenol-D particles within a shape-memory alloy matrix to create a ferromagnetic shape-memory composite with combination of the characteristics of shape-memory alloys and magnetostrictive materials. The Terfenol-D particles will be elongated by about 0.1% when applying a magnetic field. The generated force is high enough to induce the martensitic transformations in the matrix at appropriate temperatures. Therefore, the orientation and growth of the martensite plates may be controlled by the magnetic field,

and by the distribution and properties of the Terfenol-D particles embedded in the matrix. The magnetic control of the shape-memory effect through the magnetostrictive inclusions may be used independently, or simultaneously with the thermal control to achieve optimal performance. Experimentally, a Terfenol-D/Cu–Zn–Al composite was prepared using Cu–Zn–Al SMA and Terfenol-D (15 wt%) powders with the shock-wave compaction method [101]. However, the magneto(visco)elastic response and thermomechanical properties of the composite have not been reported. Most probably, this kind of composite is not suitable as an active actuator material due to some technical limitations.

As an alternative, the high passive-damping capacity of the magnetic powders/SMA matrix composites may be utilized. It is known that Cu–Zn–Al SMAs have high damping capacity at large strain amplitudes due to thermoelastic martensitic transformations, but their stiffness is inadequate for some structural applications. On the other hand, the ferromagnetic alloys including Terfenol-D, Fe–Cr, Fe–Cr–Al and Fe–Al are known to have relatively high strength as well as high damping capacity in the range of small strain amplitudes, and low damping capacity in the range of large strain amplitudes. In principle, the combination of Cu–Zn–Al matrix and ferromagnetic alloy inclusions should yield high damping capacity over a wide range of strain amplitudes, and higher stiffness than that of the monolithic Cu–Zn–Al alloys. Accordingly, three kinds of metal matrix composites were fabricated from prealloyed Cu–26.5 wt% Zn–4.0 wt%Al powders (as a matrix) and rapidly solidified Fe–7 wt%Al, Fe–20 wt%Cr and Fe–12 wt%Cr–3 wt%Al alloy flakes (30 vol%), respectively, by powder metallurgy processing [102]. The interfaces between the Cu–Zn–Al matrix and the flakes in the consolidated composites were delineated and were free of precipitates or reaction products. In all three composites, the overall damping capacity with the strain in the range from 1.0×10^{-4} to 6.0×10^{-4} were found to show substantial improvements. In particular, the Fe–Cr flakes/Cu–Zn–Al composite demonstrated the highest overall damping capacity and exhibited an additional damping peak at strain 165×10^{-6} [102].

4. Hybrid composites based on thin-film shape-memory alloys

4.1. SMA/Si heterostructures

The development of shape-memory alloy thin films for microelectromechanical systems (MEMS) is one of the most important attempts which have been directed towards the engineering applications of shape-memory alloys during the past decade [9]. Owing to the extensive use in IC microfabrication technologies, silicon is particularly preferable as the substrate to fabricate and pattern SMA thin films in batches. Ti–Ni, Ti–Ni–Cu and other kinds of SMA films have been deposited onto both single-crystal silicon and polysilicon substrates [109–116].

From a thermodynamical point of view, Ti–Ni is unstable as compared to Si [109, 110, 113]. As a result, interface diffusion and chemical interactions may occur and titanium and nickel silicides may be formed on post-deposition annealing, especially at higher temperatures, of the SMA films. A thin buffer layer of niobium or gold can prevent the interdiffusion [109, 111]. In particular, a buffer layer of SiO_2 has proved to be an effective diffusion barrier and an excellent transition layer favouring the interface adherence [109, 111, 112].

The delamination of the deposited SMA films from silicon arising from the evolution of the intrinsic residual stress, must be prevented. Wolf and Heuer [116] reported that the adherence of Ti–Ni to a bare silicon wafer can be improved if it has been cleaned and etched with a buffered oxide etchant ($H_2O + NH_4F + HF$) prior to deposition. Also, modest heating of the substrate under vacuum to around 473 K, prior to deposition, can minimize contamination and improve adherence. Krulevitch *et al.* [111] also reported that *in situ* heated Ti–Ni–Cu SMA films adhere well to bare silicon. The adherence of Ti–Ni film to both bulk SiO_2 and thermal oxide coated silicon (SiO_2/Si) were reported to be excellent. A 50–300 nm thick layer of Ti–Ni with parent B2 phase which remains untransformed was observed adjacent to the interface. The untransformed interlayer, which may be due to the effect of the strong (1 1 0) B2 texture, contributes to the interface adherence by accommodating the strain through a gradient or by absorbing the elastic energy [112, 114]. In some cases, electrical isolation of the film is needed. Wolf and Heuer [116] reported that deposition of a 0.1 μm polysilicon layer on SiO_2 prior to deposition of Ti–Ni resulted in a well-bonded interface.

The structure of the composite films should be properly designed to achieve optimal performance. Owing to the mechanical constraints via the interface, the substrate stiffness, determined by the film/substrate thickness ratio, has a significant effect on the transformation characteristics of the SMA layer and on the output energy of the composite multilayers [112, 114]. The stress and its evolution in the bimorph films is governed by Equations 1 and 2 in [9]. While, the tip deflection, δ, of the diaphragm cantilever is given by [111]

$$\delta = \frac{3E_s\sigma_{rec}t_s t_f(t_s + t_f)l^2}{E_s^2 t_s^4 + E_f t_s(4t_s^3 t_f + 6t_s^2 t_f^2 + 4t_s t_f^3) + E_f^2 t_f^4} \quad (5)$$

where l is the cantilever length and σ_{rec} the recoverable stress and the other symbols are defined in the same way as in Equations 1 and 2 in [9]. The optimum SMA film thickness for maximum cantilever deflection depends on the relative stiffness of the SMA film and the underlying beam [111]. The behaviour of the film depends on the film thickness and approaches bulk behaviour as the film becomes a few micrometres thick. However, more complaint actuating films must be slightly thicker for maximum tip deflection [111, 114]. Up to now, some novel microdevices using the SMA/Si diaphragm have been patterned and fabricated, such as microvalves and microactuators [117–120], micro robot arm [121] and microgripper [111, 122].

4.2. SMA/piezoelectric heterostructures

An ideal actuation material would display a large stroke, high recovery force and superior dynamical response. Shape-memory alloys exhibit large strokes and forces but suffer from a slow response. Ferroelectric ceramics are very sensitive to applied stresses through the direct piezoelectric effect and generate powerful forces by means of the converse piezoelectric effect. The ceramics are characterized by excellent dynamical response (of the order of microseconds), but their displacements are quite small (of the order of a few micrometres) due to their small strain magnitude ($< 10^{-3}$) [4, 123, 124]. There is a large number of ferroelectric ceramics, but the most widely investigated and currently applied for thin-film technology are the titanate and niobate (with oxygen octahedral structure) types, such as lead titanate ($PbTiO_3$), lead zirconate titanate (PZT), lead lanthanum zirconate (PLZT), barium titanate ($BaTiO_3$) and strontium titanate ($SrTiO_3$) [110, 123–126]. By combining ferroelastic SMAs with ferroelectric piezoelectric ceramics, some hybrid heterostructures can be fabricated which may have the optimum characteristics of both materials.

Piezoelectric thin films can be fabricated with various techniques such as sputtering, chemical vapour deposition (CVD) and sol–gel processing. The sol–gel process of piezoceramics has had increasing applications because the chemical composition can be controlled precisely [110, 124, 125]. Of particular concern here is whether the amorphous piezoelectric materials can be synthesized on SMA or vice versa. Chen *et al.* [127] first successfully deposited thin films of PZT and PLZT, 0.6 and 1.4 μm in thickness, respectively, on Ti–Ni SMA foils by the sol–gel process and multistep spin-on coating techniques. The amorphous films were annealed at temperatures above 773 K to obtain the perovskite phases. The dielectric constant and loss tangent at 100 kHz of the Ti–Ni/PZT composite film were about 700 and 0.03, respectively, comparable to that of the bulk ceramics. The PZT films were found to adhere well to the Ti–Ni alloy for strains as large as 0.4%, and their ferroelectric properties remain unchanged during repeated cycling through the shape-memory transformation. However, considerable cracking was observed when the diaphragms were subjected to a strain of 0.5% [127]. Jardine and Mercado [110, 128–132] and Alam *et al.* [133] also successfully deposited the thin films of PZT, $BaTiO_3$ and $SrTiO_3$ on to commercially available Ti–Ni SMA bulk and thin films by sol–gel and spin-on techniques or with the pulsed-laser deposition method, although the quality of the multilayer composites were not so desirable.

It is very important that the fabrication steps be minimized and, if deposited on amorphous SMA films, both types of the amorphous thin films be crystallized simultaneously, so as not to promote degradation of performance due to second phases and chemical interactions via diffusion. The composite multilayers were annealed at various temperatures ranging from 723–973 K and a suitable crystallization temperature was found at about 873 K [113]. Although the heterostructures have good SME and piezoelectric properties, the cracking of the piezoceramic thin-film layer remains a crucial problem. Generally, a thicker PZT film causes more cracks than a thinner film, whereas a smooth surface roughness and a slow cooling rate after annealing will favour the bonding of the PZT film to the Ti–Ni SMA substrate [128]. An effective method to lessen cracking is to deposit a buffer layer of TiO_2 on Ti–Ni SMA foil and then deposit the piezoelectric film on the TiO_2/Ti–Ni substrate [110, 112, 128]. Nevertheless, how to accommodate the stress and dynamical coupling of the dissimilar material layers remains a crucial problem to be solved before they can be employed for actuation application.

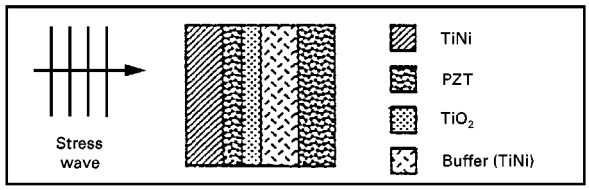

Figure 13 Schematic illustration of a smart ferroelastic–ferroelectric heterostructure for active damping [128].

Alternatively, the ferroelastic–ferroelectric heterostructures may be effective for active suppression of high-amplitude acoustic waves and shock waves [128–132]. By coupling Ti–Ni SMA to PZT via a TiO_2 layer, the final composite material can sense and actuate to dampen structural vibration without the use of external control. The mechanism of the active damping can be explained by considering an approaching stress wave, as shown in Fig. 13. The stress wave propagates through the Ti–Ni SMA, producing a stress-induced martensitic transformation where some of the mechanical energy is converted into heat. The wave further produces a voltage across the first ferroelectric layer that can be used to produce an out-of-phase stress wave by the second ferroelastic layer and, in turn attenuate the stress wave. A mechanical metallic impedance buffer (such as aluminium, titanium and Ti–Ni) is used to provide time for the counter-stress actuation to occur [128–132].

4.3. SMA/Terfenol-D heterostructures

Magnetostrictive materials with either crystalline or amorphous structure provide higher counterforces and up to 20 times higher strains than piezoelectric ceramics [134–136]. Of the magnetrostrictive materials presently available, the compounds Terfenol-D ($Tb_xDy_{1-x}Fe_2$), have the largest magnetostriction and magnetization at room temperature, the strain output being up to 0.2% when subjected to up to 2500 Oe, and in some cases approaching 1%. The alloys are analogous to electrostrictive materials in that they respond quadratically to an applied field. The optimum performance of Terfenol-D is achieved with the combination of a bias field plus a bias compressive stress. The superior properties of Terfenol-D have attracted increasing attention to the use of this

material in both bulk and thin-film form, applied for actuation [112, 134–136].

Terfenol-D films can also be fabricated with the conventional magnetron sputtering techniques. Su *et al.* [112, 137–141], Quandt *et al.* [142, 143] and other researchers [144–146] have successfully deposited Terfenol-D films of various thickness on to Si/SiO_2 substrates by d.c. magnetron sputtering. The thin films deposited at room temperature are amorphous and the crystallization temperatures are much higher (> 903 K). However, it should be remembered that the as-received amorphous Terfenol-D films are excellent ferromagnetic materials. The amorphous films show a sharp increase in the magnetostriction at low magnetic fields and no hysteresis during cycling of the field, whereas the crystalline films exhibit magnetostrictive hysteresis loops and large remanence and coercivity which limit their application [138]. Because the amorphous Terfenol-D films do not involve annealing at elevated temperatures which may address undesirable chemical interactions or diffusion, the fabrication of hybrid composite films seems easier and more simple. For instance, the Terfenol-D films can be grown on crystalline Ti–Ni SMA bulk or deposited-films annealed before the sputtering of the Terfenol-D films. Su *et al.* [114] proposed the concept of a Terfenol-D/Ti–Ni/Si composite in which the ferroelastic actuation can be triggered by a magnetic field. The Terfenol-D/SiO_2/Si and Ti–Ni/SiO_2/Si composites have been fabricated and characterized [114], but no further reports on the successful fabrication of Terfenol-D/Ti–Ni hybrid composite films are recorded in the open literature. Surely, this is an interesting and exciting subject that needs further investigations and, of course, some technical challenges, such as the interface compatibility, still remain ahead.

5. Conclusion

Various kinds of smart hybrid composites can be designed by incorporating shape-memory material components with other advanced materials. The shape-memory hybrid composites show some unique properties or functions such as self-strengthening, active modal modification, high damping, damage resistance and control, which can be utilized to tailor or tune the overall performance of a smart structural system. Thanks to the numerous efforts and exploratory approaches made by many researchers, during the past decade the shape-memory hybrid composites have evolved and become one of the promising advanced composites for smart systems. However, the research and development of the smart composites is still in its initial stage; many problems remain unresolved and some technical challenges lie ahead. One of the key problems of particular concern is to develop novel interfacial technology to bind shape-memory materials with dissimilar components. To achieve a multilayered or gradient interface which provides durability, mechanical stability, dynamical coupling, chemical and physical compatibility, will be the very demanding objective. For shape-memory material components, a well-bonded interface will constrain the martensitic transformations and hence sacrifice the shape-memory effect and other performance. Therefore, a compromise should be reached to achieve optimal overall performance of the composite system. Unfortunately, the phase transformation characteristics under various constraints exerted by coupled components via the interface, including the phase stability, ageing or degradation and transformation hysteresis, are not well understood so far. The next task is to gain a better understanding to model the potential emergent properties of the complex systems with the non-linear integration effects of the components. Fortunately, a variety of established models describing the constitutive relations of SMA hybrid composites [20, 25, 103–108] have shed light on the future approach directions. The numerical modelling and computer simulations of the composites, in combination with some experimental characterization efforts, will further lead to the optimization of technical factors such as structural configuration, geometry, processing procedures and selection of component materials, and, in turn, the improvement of the overall performance of the smart composites.

Acknowledgements

The authors thank Mr J. Cederstrom, Dr L. S. Cui and Dr W. J. Tang for their critical reading of the manuscript and helpful discussion. We also thank Professor K. Inoue and M. Taya and Dr W. D. Armstrong for the papers they provided prior to publication.

References

1. C. A. ROGERS, in "Smart Materials, Structures, and Mathematical Issues", edited by C. A. Rogers (Technomic, Lancaster, 1989) p. 221.
2. C. A. JAEGAR and C. A. ROGERS, *ibid.*, p.14.
3. B. Z. JANG, in "Proceedings of the International Conference on Advanced Composite Materials", edited by T. Chandra and A. K. Dhingra (TMS, Warrendale, 1993) p. 661.
4. M. V. GANDHI and B. S. THOMPSON, in "Smart Materials and Structures" (Chapman and Hall, London, 1992) p.70.
5. C. A. ROGERS, in "US–Japan Workshop on Smart/Intelligent Materials and Systems", edited by I. Ahmad *et al.* (Technomic, Lancaster, 1990) p.11.
6. *Idem*, in "Proceedings of the American Society of Composites 3rd Technical Conference on Composite Materials" (Technomic, Lancaster, 1988) p.719.
7. *Idem*, *J. Acoust. Soc. Am.* **88** (1990) 2803.
8. J. S. N. PAINE and C. A. ROGERS, in "Adaptive Structures and Composite Materials: Analysis and Application", edited by E. Garcia *et al.*, AD-Vol. 45/MD, Vol. 54 (ASME, New York, 1994) p.37.
9. Z. G. WEI, R. SANDSTRÖM and S. MIYAZAKI, *J. Mater. Sci.* **33** (1998).
10. E. HORNBOGEN, M. THUMANN and B. VELTEN, in "Progress in Shape-Memory Alloys", edited by S. Eucken (DGM, Informationsgesellschaft, Verlag, 1992) p. 225.
11. K. ESCHER and E. HORNBOGEN, *J. Phys. IV* **1** (1991) C4–427.
12. R. BARRETT and R. S. GROSS, *Smart Mater. Struct.* **5** (1996) 255.
13. S. TROMBERT, J. CHAZELAS, P. BONNIAU, W. VAN MOORLEGHEM, M. CHANDRASEKARAN and J. F. SILVAIN, in "Proceedings of the Third International Conference on Intelligent Materials", edited by P. F. Gobin and J. Tatibouet, Vol. 2779 (SPIE, Lyon, 1996) p.475.

14. Y. FURUYA, A. SASAKI and M. TAYAL, *Mater. Trans. JIM* **34** (1993) 224.
15. Y. FURUYAL, *J. Intelligent Mater. Systems Struct.* **7** (1996) 321.
16. M. TAYA, Y. FURUYA, Y. YAMADA, R. WATANABE, S. SHIBATA and T. MORI, in "Smart Structures and Materials 1993: Smart Materials", edited by V. Varadan, Vol. 1916 (SPIE, Orlando, 1993) p. 373.
17. Y. FURUYA and M. TAYA, *J. Jpn Inst. Metals* **60** (1996) 1163.
18. W. D. ARMSTRONG and H. KINO, *J. Intelligent Mater. Systems Struct.* **6** (1995) 809.
19. W. D. ARMSTRONG and T. LORENTZEN, *Scripta Mater.* **36** (1997) 1037.
20. W. D. ARMSTRONG, *J. Intelligent Mater. Systems Struct.* **7** (1996) 448.
21. J. H. LEE, K. HAMADA, K. MIZIUUCHI, M. TAYA and K. INOUE, in "Proceedings of MRS 1996 Fall Meeting", in press.
22. K. MIZUUCHI, K. YAMAUCHI, K. HAMADA, K. INOUE, M. TAYA and K. ENAMI, *J. Jpn Instit. Metals* **61** (1997) 727.
23. B. FILES and G. B. OLSON, in "Proceedings of the 2nd International Conference on Shape Memory and Superelastic Technologies", edited by A. Pelton, D. Hodgson, S. Russell and T. Duerig (SMST, Fremont, 1997) p.281.
24. C. A. ROGERS, C. LIANG and J. JIA, *Computers Struct.* **38** (1991) 569.
25. J. JIA and C. A. ROGERS, *J. Mech. Design* **114** (1992) 670.
26. A. BAZ, S. POH, J. RO, M. MUTUA and J. GILHEANY, in "Intelligent Structural Systems", edited by H. S. Tzou and G. L. Anderson (Kluwer Academic, Dordrecht, 1992) p. 169.
27. J. EPPS and R. CHANDRA, "Smart Structures and Materials 1995: Smart Structures and Integrated Systems", edited by I. Chopra, SPIE Vol. 2443 (SPIE, San Diego, 1995) p.76.
28. J. S. N. PAINE and C. A. ROGERS, in "Active Materials and Smart Structures", edited by G. L. Anderson and D. C. Lagoudas, SPIE, Vol.2427 (SPIE, College Station, 1994) p. 358.
29. T. C. KIESLING, Z. CHAUDHRY, J. S. N. PAINE and C. A. ROGERS, in "Proceedings of the 37th AIAA/ASME/ASCE/AHS/ASC Structures, Structural Dynamics, and Materials Conference", Salt Lake City, UT (ASME, New York, 1996) p. 1448.
30. J. S. N. PAINE and C. A. ROGERS, "Smart Structures and Materials 1994: Smart Structures and Intelligent Systems", edited by N. W. Hagood, SPIE, Vol. 2190 (SPIE, Orlando, 1994) p. 402.
31. *Idem*, *J. Thermoplast. Compos. Mater.* **4** (1991) 102.
32. D. A. HEBDA, M. E. WHITLOCK, J. B. DITMAN and S. R. WHITE, *J. Intelligent Mater. Systems Struct.* **6** (1995) 220.
33. A. BAZ and J. RO, *Compos. Engi.* **2** (1992) 527.
34. S. R. WHITE, M. E. WHITLOCK, J. B. DITMAN and D. A. HEBDA, in "Adaptive Structures and Material Systems", edited by G. P. Carman and E. Garcia, AD-Vol. 35 (ASME, New York, 1993) p. 71.
35. J. S. N. PAINE and C. A. ROGERS, *ibid*, p. 63.
36. K. JONNALAGADDA and N. R. SOTTOS, "Smart Structures and Materials 1995: Mathematics and Control in Smart Structures", edited by V. V. Varadan, SPIE, Vol. 2442 (SPIE, San Diego, 1995) p. 143.
37. W. J. ELSPASS and J. KUNZMANN, "Smart Structures and Materials 1996: Smart Structures and Integrated Systems", edited by I. Chopra, SPIE, Vol. 2717 (SPIE, San Diego, 1996) p. 320.
38. J. GRANDO and M. SALVIA, in "Proceedings of the Third International Conference on Intelligent Materials", edited by P. F. Gobin and J. Tatibouet, SPIE, Vol. 2779 (SPIE, Lyon, 1996) p. 530.
39. J. E. BIDAUX, J. A. E. MANSON and R. GOTTHARDT, in "Proceedings of the First International Conference on Shape Memory and Superelastic Technologies", edited by A. R. Pelton, D. Hodgson and T. Duerig (SMST, Fremon, 1994) p.37.
40. J. E. BIDAUX, J. A. MANSON and R. GOTTHARDT, in "Proceedings of the 2nd International Conference on Shape Memory and Superelastic Technologies", edited by A. Pelton, D. Hodgson, S. Russell and T. Duerig (SMST, Fremon, 1997) p. 287.
41. K. JONNALAGADDA, G. E. KLINE and N. R. SOTTOS, *Exp. Mech.* **37** (1997) 78.
42. S. M. MENG, T. J. QING and B. Q. TAO, *Mech. Practice* **17**(4) (1995) 16 (in Chinese).
43. A. BAZ, K. IMAM and J. MCCOY, *J. Sound Vib.* **140** (1990) 437.
44. C. LIANG and C. A. ROGERS, *J. Vib. Acoustics* **115** (1993) 129.
45. C. A. ROGERS, C. R. FULLER and C. LIANG, *J. Sound Vib.* **136** (1990) 164.
46. C. LIANG, C. A. ROGERS and C. R. FULLER, *ibid.* **145** (1991) 23.
47. L. MCD. SCHETKY, C. LIANG and C. A. ROGERS, "Smart Structures and Materials 1994: Smart Structures and Intelligent Systems", edited by N. W. Hagood, SPIE Volume 2190 (SPIE, Orlando, 1994) p. 422.
48. C. A. ROGERS and C. LIANG, (1990), unpublished work.
49. J. J. EPPS and R. CHANDRA, "Smart Structures and Materials 1996: Smart Structures and Integrated Systems", edited by I. Chopra, SPIE Vol. 2717 (SPIE, San Diego, 1996) p. 101.
50. V. BABURAJ and Y. MATSUZAKI, *J. Intelligent Mater. Systems Struct.* **5** (1994) 647.
51. *Idem*, *ibid.* **7** (1996) 427.
52. W. R. SAUNDERS, H. H. ROBERTSHAW and C. A. ROGERS, *ibid.* **2** (1991) 508.
53. Z. CHAUDHRY and C. A. ROGERS, *ibid.* **2** (1991) 581
54. *Idem*, *J. Mech. Design* **114** (1992) 343.
55. A. BAZ, T. CHEN and J. RO, "Smart Structures and Materials 1994: Smart Structures and Intelligent Systems", edited by N. W. Hagood, SPIE Vol. 2190 (SPIE, Orlando, 1994), p. 436.
56. D. C. LAGOUDAS and I. G. TADJBAKSH, *smart Mater. Struct.* **1** (1992) 162.
57. Z. BO and D. C. LAGOUDAS, "Smart Structures and Materials 1994 : Smart structures and Intelligent Systems", edited by N. W. Hagood, SPIE Vol. 2190 (SPIE, Orlando, 1994) p. 495.
58. H. J. PFAEFFLE, D. C. LAGOUDAS, I. G. TADJBASKSH and K. C. CRAIGI, "Smart structures and Intelligent Systems", edited by V. Varadan, SPIE Vol. 1917 (SPIE, Orlando, 1993) p. 762.
59. M. SHAHINPOOR and G. WANGI, Smart structures and Material 1995: Industrial and Commercial Applications of Smart Structures Technologies", edited by V. Varadan, SPIE Vol. 2447 (SPIE, San Diego, 1995) p. 291.
60. G. WANG and M. SHAHINPOOR, "Smart Structures and Materials 1996: Mathematics and Control in Smart Structures", edited by V. V. Varadan, SPIE Vol. 2715 (SPIE, San Diego, 1996) p. 51.
61. P. M. TAYLOR, K. G. SWIFT, A. J. CREED and R. S. KALAWSKY, in "Proceedings of the 5th International Conference on Adaptive Structures, edited by J. Tani, E. J. Breitbach, B. K. Wada and S. Chonan (Technomic, Lancaster, 1994) p. 238.
62. C. LIANG, F. DAVIDSON, L. M. SCHETKY and F. K. STRAUB, "Smart Structures and Materials 1996: Smart Structures and Integrated Systems", edited by I. Chopra, SPIE Vol. 2717 (SPIE, San Diego, 1996) p. 91.
63. L. C. BRINSON, M. S. HUANG, C. BOLLER and W. BRAND, *J. Intelligent Mater. Systems Struct.* **8** (1997) 12.
64. A. R. SHAHIN, P. MECKL and J. D. JONES, *ibid.* **8** (1997) 51.
65. H. YOSHIDA, *Adv. Compos. Mater.* **5** (1995) 1.
66. H. YOSHIDA, A. FUNAKI and S. YANO, "Proceedings of the 3rd International Conference on Intelligent Materials", edited by P. F. Gobin and J. Tatibouet, SPIE Vol. 2779 (SPIE, Lyon, 1996) p. 523.
67. A. V. SRINIVASAN, D. M. MCFARLAND, H. A. CARNISTRARO and E. K. BEGG, *ibid.*, p. 700.

68. J. S. N. PAINE and C. A. ROGERS, *J. Intelligent Mater. Systems Struct.* **6** (1995) 210.
69. J. S. N. PAINE and C. A. ROGERS, "Smart Structures and Materials 1995: Smart Structures and Integrated Systems", edited by I. Chopra, SPIE 2443 (SPIE, San Diego, 1995) p. 195.
70. C. M. FRIEND and N. B. MORGAN, "Proceedings Second European Conference on Smart Structures and Materials", edited by A. McDonach *et al*., SPIE Vol. 2361 (SPIE, Glasgow, 1994) p. 94.
71. *Idem*, *J. Phys. IV* **5** (1995) C2- 415.
72. C. M. FRIEND, A. P. ATKINS and N. B. MORGAN, *ibid.* **5** (1995) C8-1171.
73. C. J. DORAN In "Proceedings of the Second European Conference on Smart Structures and Materials", edited by A. McDonach *et al*., SPIE Vol. 2361 (SPIE, Glasgow, 1994) p. 98.
74. C. A. ROGERS, C. LIANG and S. LI, in "Proceedings of the AIAA 32nd Structures, Structural Dynamics and Materials Conference" AIAA-91-1145-CP (ASME, Baltimore, 1991) p. 1190.
75. Y. L. DU and J. X. NIE, *Progr. Mech.* **24** (1994) 499 (in Chinese).
76. J. S. N. PAINE and C. A. ROGERS, *J. Intelligent Mater. Systems Struct.* **5** (1994) 530.
77. *Idem*, Adaptive in Structures and Composite Materials: Analysis and Application", edited by E. Garcia, H. Cudney and A. Dasgupta, AD-Vol. 45/MD-Vol. 54 (ASME, New York, 1994) p. 75.
78. R. L. ELLIS, F. LALANDE, H. JIA and C. A. ROGERS, in "Proceedings 38th AIAA/ASME/ ASCE/AHS/ASC Structures, Structural Dynamics, and Materials Conference", Kissimmee, FL, (ASME, New York, 1997), in press.
79. H. JIA, F. LALANDE, R. L. ELLIS and C. A. ROGER, *ibid.* (1997) in press.
80. R. L. ELLIS, Master thesis, Virginia Polytechnic Institute and State University (1996).
81. T. FUKUDA, N. OHSHIMA and K. HOURAI, in "Proceedings of the 9th International Conference on Composite Materials/Composites Design", edited by A. Miravete, Madrid, Spain, (Woodhead Publ., Zaragoza, 1993) p. 323.
82. C. LIANG, C. A. ROGERS and E. MALAFEEW, "Smart Structures and Materials", edited by G. K. Haritos, AD-Vol. 24/AMD-Vol. 123 (ASME, New York, 1991) p. 97.
83. E. J. LAVERNIA, R. J. PEREZ and J. ZHANG, *Metall. Mater. Trans.* **26A** (1995) 2803.
84. Y. YAMADA, M. TAYA and R. WATANABE, *Mater. Trans. JIM* **34** (1993) 254.
85. L. S. CUI, PhD dissertation, Dalian University of Technology (1994).
86. K. OTSUKA, in "Shape Memory Material '94", edited by Y. Chu and H. Tu (International Academic, Beijing, 1994) p. 129.
87. S. ZHANG, L. LU and M. O. LAI, *Mater. Sci. Eng.* **A171** (1993) 257.
88. Z. G. WEI, C. Y. TANG, W. B. LEE, L. S. CUI and D. Z. YANG, *Mater. Lett.* **32** (1997) 313.
89. S. TROMBERT, J. CHAZELAS, P. BONNIAU, W. VAN MOORLEGHEM, M. CHANDRASEKARAN and J. F. SILVAIN, in "Proceedings of the 3rd International Conference on Intelligent Materials", edited by P. F. Gobin and J. Tatibouet, SPIE Vol. 2779 (SPIE, Lyon, 1996) p. 475.
90. J. VAN HUMBEECK, *ibid.* (1997) p. 442.
91. L.LU, M. O. LAI, Y. B. LIU and S. C. LIM, in "Proceedings of the 9th International Conference on Composite Materials: Ceramic Matrix Composites and other Systems", edited by A. Miravete (Woodhead Publ., Zaragoza, 1993) p. 419.
92. V. E. PANIN, A. I. SLOSMAN, B. B. OVECHKIN, M. P. BONDAR and M. P. BONDAR and N. A. KOSTYUKOV, *Sov. Powder Matall. Metal Ceramics.* **24** (1985) 526.
93. S. N. KUL'KOV, T. M. POLETIKA, A. YU. CHUKHLOMIN and V. E. PANIA, *ibid.* **23** (1984) 652.
94. D. MARI and D. C. DUNAND, *Metall. Mater. Trans.* **26A** (1995) 2833.
95. K. L. FUKAMI-USHIRO, D. MARI and D. C. DUNAND, *ibid.* **27A** (1996) 183.
96. K. L. FUKAMI-USHIRO, and D. C. DUNAND, *ibid.* **27A** (1996) 193.
97. D. C. DUNAND D. MARI, M. A. M. BOURKE and J. A. ROBERTS, *ibid.* **27A** (1996) 2820.
98. L. SANDLUND and T. CEDELL, in "Transducers for Sonics and Ultrasonics", edited by M. D. McCollum, B. F. Harmonic and O. B. Wilson (Technomic, Orlando, FL, 1992) p. 113.
99. L. SANDLUND, M. FAHLANDER, T. CEDELL, A. E. CLARK, J. B. RESTORFF and M. WUN-FOGLE, *J. Appl. Phys.* **75** (1994) 5656.
100. K. ULLAKKO, P. G. YAKOVENKO and V. G. GAVRILJUK, "Small Structures and Materials 1996: Mathematics and Control in Smart Structures", edited by V. V. Varadan, SPIE Vol. 2715 (SPIE, San Diego, 1996) p. 42.
101. K. ULLAKKO, in "Proceedings of the 3rd International Conference on Intelligent Materials", edited by P. F. Gobin and J. Tatibouet, SPIE Vol. 2779 (SPIE, Lyon, 1996) p.505.
102. K. SHIN, C. R. WONG and S. H. WHANG, *Mater. Sci. Eng.* **A165** (1993) 35.
103. B. J. SULLIVAN, *J. Intelligent Mater. Systems Struct.* **5** (1994) 825.
104. J. G. BOYD and D. C. LAGOUDAS, *Int. J. Plasticity* **12** (1996) 843.
105. *Idem*, *J. Intelligent Mater. Systems Struct.* **5** (1994) 333.
106. R. STALMANS, J. VAN HUMBEECK and L. DELAEY, in "Proceedings of the 3rd International Conference on Intelligent Materials", edited by P. F. Gobin and J. Tatibouet, SPIE Vol. 2779 (SPIE, Lyon, 1996) p. 511.
107. W. WU, F. GORDANINEJAD and R. A. WIRTZ, *J. Intelligent Mater. Systems Struct.* **7** (1996) 441.
108. H. JIA, F. LALANDE and C. A. ROGERS, "Review of Constitutive Modeling of Shape Memory Alloys", Research Report, VPI&SU (1996).
109. A. P. JARDINE, J. S. MADSEN and P. G. MERCADO, *Mater. Charact.* **32** (1994) 169.
110. A. P. JARDINE, *Mater. Res. Soc. Symp. Proc.* **276** (1992) p. 31.
111. P. KRULEVITCH, A. P. LEE, P. B. RAMSEY J. C. TREVINO, J. HAMILTON and M. A. NORTHRUP, *J. Microelectromech. Systems* **5** (1996) 270.
112. Q. SU, T. KIM, Y. ZHENG and M. WUTTIG, "Smart Structures & Materials 1995: Smart Materials", edited by A. P. Jardine, SPIE, Vol. 2441 (SPIE, San Diego, 1995) p. 179.
113. A. P. JARDINE, *Smart Mater. Struct.* **3** (1994) 140.
114. Q. SU, T. KIM, Y. ZHENG and M. WUTTIG, unpublished report (1994).
115. D. S. GRUMMON, LI HOU, Z. ZHAO and T. J. PENCE, *J. Phys. IV*. **5-C8** (1995) 665.
116. R. H. WOLF and A. H. HEUER *J. Microelectromech. Systems* **4** (1995) 206.
117. A. D. JOHNSON, J. D. BUSCH, C. A. RAY and C. SLOAN, *Materi. Res. Soc. Symp. Proc.* **276** (1992) p. 151.
118. A. D. JOHNSON, J. D. BUSCH, in "Proceedings of the 1st International Conference on Shape Memory and Superelastic Technologies", edited by A. R. Pelton, D. Hodgson and T. Duerig (SMST, Fremon, 1994) p. 299.
119. A. D. JOHNSON and V. V. MARTYNOV in "Proceedings of the 2nd International Conference on Shape Memory and Superelastic Technologies", edited by A. R. Pelton, D. Hodgson and T. Duerig (SMST, Fremon, 1997) p. 149.
120. C. A. RAY, C. L. SLOAN, A. D. JOHNSON, J. D. BUSCH and B. R. PETTY, *Mater. Res. Soc. Symp. Proc.* **276** (1992) 161
121. K. KURIBAYASHI, T. TANIIGUCHI, M. YOSITAKE and S. OGAWA, *ibid*., p. 167.
122. M. MERTMANN, E. HORNBOGEN and K. ESCHER, in "Shape Memory Materials'94", edited by Y. Chu and H. Tu (International Academic, Beijing, 1994) p. 556.
123. L. E. CROSS, in "Ferroelectric Ceramics", edited by N. Sotter and E. L. Colla, (Birkhäuser, Basel, 1993) p. 1.
124. J. F. SCOTT, *ibid.* p. 185.
125. K. SREENIVAS, *ibid*., p. 213.

126. A. M. FLYNN, L. S. TAVROW, S. F. BART, R. A. BROOKS, D. J. EHRLICH, K. R. UDAYAKUMAR and L. E. CROSS, *J. Microelectromech. Systems* **1** (1992) 44.
127. J. CHEN, Q. C. XU, M. BLASZKIEWICZ, R. MEYER JR and R. E. NEWNHAM, *J. Am. Ceram. Soc.* **75** (1992) 2891.
128. P. G. MERCADO and A. P. JARDINE, in "Proceedings of the 2nd International Conf. on Intelligent Materials", edited by C. A. Rogers and G. G. Wallace (Technomic, Lancaster, 1994) p. 665.
129. *Idem*, *Mater. Res. Soc. Symp. Proc.* **360** (1995) 287.
130. *Idem*, *ibid*., p. 419.
131. *Idem*, in "Smart Structures and Materials 1994: Smart Materials", edited by V. K. Varadan, SPIE, Vol. 2189 (SPIE, Orlando, 1994) p. 26.
132. A. P. JARDINE and P. G. MERCADO, *ibid*., p. 37.
133. M. R. ALAM, A. KUMAR, N. SHU, H. L. CHAN and Q. YOU, *Appli. Surf. Sci.* **109**/**110** (1997) 393.
134. D. C. JILES, in "New Materials and their Application 1990", edited by D. Hollan (IOP, London, 1990) p. 365.
135. A. E. CLARK, *Mater. Res. Soc. Symp. Proc.* **360** (1995) 171.
136. O. D. MCMASTERS, *J. Rare Earths* **13** (1995) 295.
137. Q. SU, S. RIBA, A. ROYTBURD and M. WUTTIG, in "Proceedings of the 2nd International Conf. on Intelligent Materials", edited by C. A. Rogers and G. G. Wallace (Technomic, Lancaster, 1994) p. 1185.
138. Q. SU, Y. ZHENG and M. WUTTIG, *Mater. Res. Soc. Symp. Proc.* **360** (1995) 195.
139. T. KIM, Q. SU and M. WUTTIG, *ibid*., p. 275.
140. Q. SU, J. MRILLO, Y. WEN and M. WUTTIG, *J. Appl. Phys.* **80** (1996) 3604.
141. Q. SU, J. P. TETER, Y. WEN J. R. CULLEN and M. WUTTIG, *ibid* **81** (1997) 5424.
142. E. QUANDT, *ibid*. **75** (1994) 5653.
143. E. QUANDT, B. GERLACH and K. SEEMANN *ibid*. **76** (1994) 7000.
144. F. SCHATZ, M. HIRSCHER, G. FLIK and H. KRONMULLER, *Phys. Statu. Solidi* (*a*) **137** (1993) 197.
145. Y. HAYASHI, T. HONDA, K. I. ARAI, K. ISHIYAMA and M. YAMAGUCHI, *IEEE Trans. Magn.* **29** (1993) 3129.
146. M. LOVELESS and S. GURUSWAMY, *J. Appl. Phys.* **79** (1996) 6222.

Received 15 September 1997
and accepted 22 April 1998